A

Dissertation

on

# Synthesis and Characterization of Molybdenum nitride ($Mo_2N$) nanopowders

*Submitted in the partial fulfilment of the requirements for award of degree of*

**Master of Science**

in

**Physics**

**(2015-2017)**


**submitted by**

Harneet Kaur Sidana

(301504016)

under the guidance of

**Dr. O. P. Pandey**

(Senior Professor)



**SCHOOL OF PHYSICS AND MATERIALS SCIENCE,**

**THAPAR UNIVERSITY**

**PATIALA (PUNJAB)-147004**


**July, 2017**

# CERTIFICATE

This is to certify that this dissertation entitled **'Synthesis and Characterization of molybdenum nitride ($Mo_2N$) nanopowders'** is submitted by **Ms. Harneet Kaur Sidana (301504016)** in fulfilment of requirement for the award of degree of Master of Science in Physics from School of Physics and Materials Science, Thapar University, Patiala, (Punjab), India. It is an exclusive record of candidate's own research work under the supervision of **Dr. O. P. Pandey**. The thesis in part or in full has not been submitted in any other university or institute for the award of any degree.

**Dr. O. P. Pandey**

(Supervisor)

Senior Professor

School of Physics and Materials Science

Thapar University, Patiala

# ACKNOWLEDGEMENT

At this moment I would like to acknowledge the people who have helped me throughout the period of past six months. Without their help and guidance I wouldn't have written this thesis.

First and foremost, I would like to thank my mentor **Dr. O. P. Pandey** (Senior Professor, School of Physics and Materials Science) for his help and support for this work. He has been always there for me, whenever I needed his help. He turned my distress into positiveness through discussion about my work. Secondly, I would like to thank **Mr. Rameez Mir** for guiding me throughout my thesis and for every in-depth discussion and analysis on the subject. To be honest I wasn't sure as to how I would complete my work but his positive attitude and dedication towards my work let me finish it off with ease. I thank him from core of my heart.

This acknowledgement is incomplete without thanking the teachers of SPMS department and the people I was around every day during these past six months. My lab mates at functional materials lab, who being intelligent and dedicated are quite funny also including **Dr. Gurbinder Kaur**, **Mr. Aayush Gupta**, **Mr. Piyush Sharma**, **Mr. Amit Singh Vig**, **Mr. Varun Singhal**, **Ms. Taranpreet Kaur** and **Ms. Ruby Priya**. Thank you all, I enjoyed a lot with you guys.

Most importantly, I would like to express my gratitude, love, and everything I owe in my life to my parents **Mr. Gurvinder pal Singh Sidana** and **Mrs. Kuldeep Kaur Sidana** and my brother **Mr. Amanpreet Singh Sidana**. Their love, concern and support inspires me and give me a boost that I can achieve anything in my life.

And above all, I would like to thank **God** for all that he has given to me and changing my tears to happiness and my fears to strength. Thank you Lord, from the bottom of my heart.

Harneet Kaur

**Harneet Kaur Sidana**

# ABSTRACT

Transition metal nitrides have gained an escalation in the recent years due to their remarkable physical and chemical properties. They have high melting point and form refractory compounds. They also possess high hardness, high wear resistance and superconductive properties. Nowadays they are also being used as catalysts. Among these nitrides, $Mo_2N$ is being extensively studied, due to its distinguishable features. $Mo_2N$ finds a wide industrial applications and catalytic activities. Taking this into account, β-$Mo_2N$ nanopowders have been synthesized in this present study via a simple reduction-nitridation technique, using ammonium heptamolybdate tetrahydrate (AHM) $(NH_4)_6Mo_7O_{24}.4H_2O$ as molybdenum source, sodium azide ($NaN_3$) as nitrogen source with magnesium (Mg) as reducing agent. Various trials were performed to obtain pure phase β-$Mo_2N$ with the variation of holding time, reaction temperature and precursor quantity. The samples were synthesized in a stainless steel (high-grade) autoclave in a pot furnace. Characterizations were done using XRD, FE-SEM and HR-TEM. It was observed that pure phase β-$Mo_2N$ was formed when precursor AHM was varied at a duration of 12 hrs while the temperature was kept at 700 $^oC$ which was confirmed by XRD pattern. FE-SEM results showed that the as synthesized samples possess platelet morphology, which was further confirmed by HR-TEM. Various factors which influences the synthesis of β-$Mo_2N$ has been discussed in the present work.

## List of Figures

**Page**

## List of Tables

**Page**

# Table of contents



## Chapter - 1

## Chapter - 2



## Chapter - 3



## Chapter - 4

# 1. Introduction

In the past few years, there has been a considerable upsurge in the research field of nitrides, which have fascinated the scientists throughout the world. Nitrides are the nitrogen-containing compounds in which nitrogen is strongly attracted to other elements through chemical bond. Nitrogen being the versatile element forms compounds with almost all the elements in periodic table, especially with metals. A special class of compounds formed between nitrogen and less electronegative elements including metals are called nitrides or metal nitrides. The nitride ion exists in two forms in nature, $N^{3-}$ (azide) and $N_2^{2-}$ which is also known as pernitride. $N^{3-}$ having the ionic radius of 140 pm, never takes part in a solution because it is highly basic and it gets protonated very fast [1]. Nitrides have attained interest due to their rich bonding schemes with more electrons localized in bonds, which is visible in their electronic as well as optical properties [2]. Nitrides are typical ceramic materials due to their high resistance to corrosion, high cohesive strength, high melting point, hardness and in some cases brittleness [3]. On the other hand, many metal nitrides are metallic conductors in which magnetic properties along with electronic properties exceed their parental metals.

The industrial demand of nitrides is increasing due to their distinctive physical and chemical properties [4]. Nitrides have also found applications in cutting tools [5], magnetic materials [6], superconductors [7], hydrotreatment catalysts [8] and coatings on the materials to provide high mechanical hardness [9]. They exhibit great strength and durability due to which they find their use in extreme conditions of temperature and pressure such as ceramic materials and therefore falls in the category of high temperature ceramics. The recent advancements in nitride chemistry has led to the increase in industrial demand of nitrides because of their refractory nature. Refractory compounds are the materials which have the ability to withstand high temperatures and have high melting point, i.e. greater than 1800 °C. They also possess high chemical stability.

From the structural view point, they are unique. The electronic structures of metal nitrides are important aspect as they also exhibit better catalytic activity as compared to those of pure elements. These materials are used as catalysts and also as catalysts support. Presently, the chemistry of nitrides mainly revolves around two themes [10]:

1. There is a huge similarity in the catalytic properties of some transition metal nitrides with that of platinum group metals.
2. The nitrides and oxynitrides possess acidic and basic properties.

There has been an incredible amount of increase in the range of application of nitrides to catalytic reactions which involves huge thermodynamic barriers arising due to making and breaking of N≡N bond. It is also seen that nitrides of s-block elements readily forms either oxides, hydroxides or ammonia when exposed to air or moisture because of their high sensitivity towards moisture. Hence, this is the dominating factor for the scarcity of nitride compounds in comparison to carbides and oxides [11]. Nitrides can be distributed into numerous categories with different physical and chemical characteristics. Although, interstitial and covalent materials only meet the refractory criteria. Nitrides of group IV, V and VI falls under this category. In material sciences, bulk metal nitrides are being used since long time, e.g. for long lasting hard coatings (e.g. TiN, ZrN, and CrN) [12], for hydrogen storage ($Li_3N$ and related nitrides [13]), and semiconductor devices (AlN, GaN, and InN) as magnetic materials [14], gas barriers and sensors [15]. Although Boron (B), Aluminum (Al), Silicon (Si) and Vanadium (Va) also form high melting point nitrides, they generally decompose at temperatures below their melting points. Among the low melting point and less stable, nitrides of Lithium (Li), Chromium (Cr), Molybdenum (Mo) and Tungsten (W) [3] are of great interest as they are used as catalysts and in coatings on different materials.

## 1.1 Classification of Nitrides

Nitrogen forms many compounds with other electropositive metals, general examples being VN, $M_3N_2$ etc. Classification of nitrides is done in five general categories based on their bonding and electronic structure which is shown in Fig.1.1.

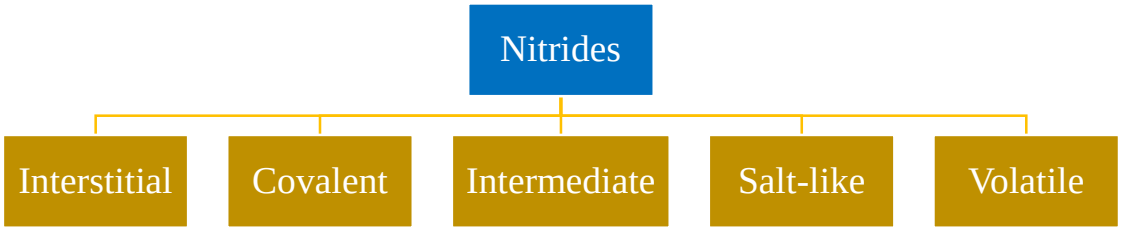


**Figure 1.1.** Classification of nitrides on the basis of bonding and electronic structure.

a) **Interstitial Nitrides:** They are formed when there is a large electronegativity and atomic size difference between host metal and nitrogen. As a result of this difference, and small size of nitrogen, it readily occupies the interstices of metal lattice. These nitrides possess metallic bonding along with few ionic and covalent bond components [21]. They also show both electronic and thermal conductivity. TMNs are categorized among the interstitial nitrides. These nitrides have wide range of properties that can be tailored to optimize the desired functionality. They rarely exhibit ideal stoichiometry. Nitrides of group IV, V and VI form interstitial nitrides such as titanium, vanadium, molybdenum and chromium etc.

b) **Covalent Nitrides:** The covalent nitrides have small electronegativity difference and small atomic radius. They largely exhibit covalent bonding. All the elements of group III such as boron, gallium, aluminum etc. forms covalent nitrides.

c) **Intermediate Nitrides:** Some elements of transition group forms intermediate nitrides because of their inability to form pure nitrides. In rare cases, some may form nitrides with some distortion in their crystal structure. Hence, these materials are highly unstable as they decompose readily. Elements such as manganese, nickel etc. forms intermediate nitrides.

d) **Salt-like/Ionic Nitrides:** The nitrides and the most electropositive element such as Li, Mg, Ca, Cd, Hg results in salt-like or ionic nitrides due to their atomic bonding which is essentially ionic. The melting points of these nitrides are very high, some of the examples include thorium nitride (ThN) ~2820 $^{o}$C, uranium nitride (UN) ~2800 $^{o}$C.

Nitrides may also be classified as:

- **Binary Nitrides** - Nitrides that contain one host metal and one nitrogen atom within the main crystal structure. e.g. TiN, VN, $Mo_2N$, TaN etc.
- **Ternary Nitrides** – Nitrides which contain two different kind of metal atoms and one nitrogen atom. They show superior thermal and diffusion barrier behavior in comparison to binary nitrides. The reason for this is disruption in the transition metal matrix crystal structure due to addition of third element. e.g. $GaFe_3N$, $AlFe_3N$ etc.
- **Quaternary Nitrides** – Nitrides that contain three different kind of metal atoms and one nitrogen atom. e.g. quaternary nitride halides $Ba_2NClI$ etc.

## 1.2 Transition Metal Nitrides (TMNs)

The elements of group IV-VI in the periodic table form transition metal nitrides (TMNs). TMNs, possess an exceptional combination of chemical, physical electrical and mechanical properties [16], due to which they are the most desirable compounds from both technological and fundamental points of view. Most of the TMNs have very low nitrogen content, and the compositions with which they are formed are often non-stoichiometric [17]. These compounds possess high hardness (comparable to that of diamond), high melting points (1700-2400 $^{o}$C) and high chemical and thermal stability. Many of the nitrides of group VI are exceptions as their decomposition temperature is relatively low as compared to that of group IV and V. Moreover, TMNs also exhibit metallic luster and show electrical and thermal conductivities of the order of same magnitude as that of pure metals. TMNs are being conventionally used under severe conditions of temperature and pressure and they also possess high durability and strength, therefore, they are used in rocket nozzles and drill bits [18]. Their hardness property is being used in ferrous alloys to provide toughness to steel, cutting tools, snow tires and golf shoe spikes. Their electrical, optical and magnetic properties have made them extremely useful for optical coatings, diffusion barriers, electrical contacts and many others [19]. Moreover, these properties of TMNs are similar to Pd, Ru (rare elements of Pt group) etc. and are promising catalysts to replace there costly noble metal catalysts for generation of clean and renewable energy [20].

## 1.3 Crystal structure and Composition

The crystal structure of most of the compounds are based on Hagg's rule [22]. According to this rule, the crystal structure depends upon the ratio of radius of non-metal atom to metal atom.

$$\text{i.e.,} \quad r = {}^{rx}/_{rm} \tag{i}$$

where, $rx$ and $rm$ are the radii of non-metal atom and metal atom respectively.

For $r > 0.59$, complicated structure of transition metal and interstitial elements are formed while for $r < 0.59$, the structure formed is mainly body centered cubic (bcc), hexagonal closed packed (hcp), face centered cubic (fcc) or simple hexagonal. In nitrides, the nitrogen being the lighter atom nests in the interstices of host metal and hence mostly form

interstitial nitrides. Most of the early transition elements act as host metal to the nitrogen because of the small $r$ values. It is also observed that the radii ratio keeps on increasing as we go from group IV to group VI [23]. Although parent metal possesses bcc structure, metal nitrides possess fcc structure. This change in structure is due to the increase in electrons because of addition of valence electrons of nitrogen atom [15]. Towards the left of the periodic table the structure of nitride resembles to those of the pure transition metals. However, towards the right, structures are more complicated. Tetragonal sites having coordination number (C.N.) = 4 and octahedral sites having C.N. = 6 are the two interstices types for bcc, fcc and hcp lattices. Most of the mononitrides having formula $MN_{1-x}$ (where M = metal) have NaCl type structure with the ABCABC sequence and C.N. = 12 having $r$ values from 0.41 to 0.59. While $MN_{1-x}$ is the most significant composition of nitrides, $M_2N$ composition is the second most important composition which follows ABAB sequence having hcp structure and a C.N. = 12. Only group V and VI show this type of structure. Simple hexagonal (hex) structure having sequence of AA or BB is another example of composition of nitrides. These structures are neither close packed nor they form octahedral sites. Such nitrides include tungsten mono-nitride (δ-WN) [21]. The nitrides of group III are crystalline in nature and exhibit wurtzite (Wz), zinc blende (ZB), and rock salt structures [24]. The wurtzite structure possess hexagonal unit cell with two lattice constants c and a, whereas, rock salt structure is only possible under extreme conditions of pressure. Fig.1.2 (a) shows fcc structure of molybdenum nitride ($Mo_2N$), where molybdenum occupies the interstitial sites and nitrogen occupy octahedral sites, and Fig.1.2 (b) shows the tetragonal structure of β-$Mo_2N$ where large spheres shows the molybdenum atom and small spheres shows the nitrogen atom.

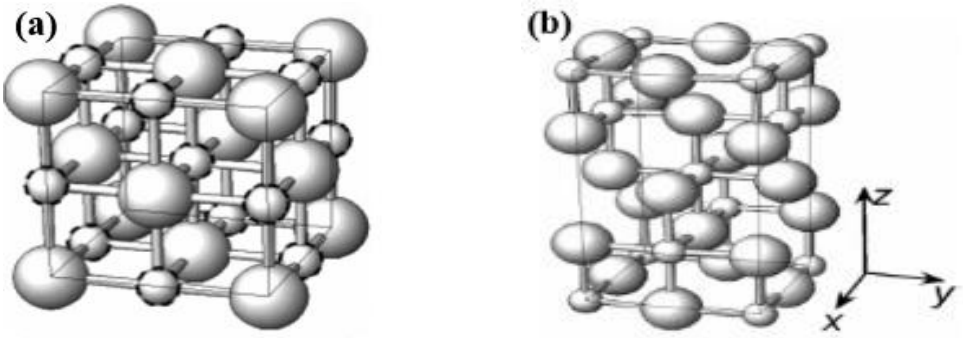


**Figure 1.2:** Crystal structure of molybdenum nitride (a) fcc structure of γ-$Mo_2N$ [25], (b) tetragonal structure of β-$Mo_2N$ [25].

Table1.1 shows the various characteristics of Group IV, V and VI nitrides on the basis of their atomic radii, composition and structure.

**Table 1.1:** Various characteristics of TMNs of Group IV, V and VI [3].

| Properties | Group IV (Ti, Zr, Hf) | Group V (V, Nb, Ta) | Group VI (Cr, Mo, W) |
|---|---|---|---|
| **Atomic radii ratio** | Lowest | Intermediate | Highest |
| **Compositions** | Mononitride | $M_2N$, MN in majority | Various compositions |
| **Structures** | fcc, hex, rhombic | hcp, fcc, hex | fcc, hcp, hex, orthorhombic |

## 1.4 Physical Properties of TMNs

### 1.4.1 Bond energy

The bond energy may be described as amount of energy needed to break apart one mole of gas. In nitrides, the more is the melting point, higher will be the bond energy. Thus, as we go from group IV to V, the metal-nitrogen bond becomes weak whereas the metal-metal bond becomes stronger. This is so because towards the right of periodic table the size of atom decreases and therefore its interatomic spacing increases.

### 1.4.2 Hardness

The hardness of nitrides of group IV to VI increases with the increase in nitrogen content. As we go from group IV-VI, the metal-$N_2$ bonding decreases. Therefore, the hardness possessed by nitrides of group IV is higher than Group V. Another factor that affects the hardness is composition of nitrides, i.e. at stoichiometry, the hardness of group IV is maximum while group V has maximum hardness before the occurrence of stoichiometry.

### 1.4.3 Density

Density of the interstitial nitrides is directly proportional to the atomic number of metal. The increase in metal to metal spacing affects the density of nitrides. The group IV nitrides have higher density as compared to their host metals. While, for group V, the nitrides have low density than their parent metal atom. Table 1.2 shows the trend followed by density of TMNs.

**Table 1.2:** Density of various TMN's [15].

| Group IV | Density (g/cm$^3$) | Group V | Density (g/cm$^3$) | Group VI | Density (g/cm$^3$) |
|---|---|---|---|---|---|
| Ti | 2000 | V | 1500 | Cr | 1100 |
| Zr | 1500 | Nb | 1400 | Mo | 1700 |
| Hf | 1600 | Ta | 1050 | W | - |

### 1.4.4 Melting point

Melting points of the nitrides is less than their corresponding carbides, with the exception of NbN, which has a higher melting point than the host metal. Also, in reference to group V, the nitrides of group IV possess higher decomposition temperature in comparison to their melting temperature. Thus, group V nitrides decompose before their melting point is attained. Table 1.3 shows the melting point of TMNs.

**Table 1.3:** Melting point of nitrides of group IV, V and VI [15].

| Group IV | Melting point (K) | Group V | Melting point (K) | Group VI | Melting point (K) |
|---|---|---|---|---|---|
| Ti | 3220 | V | 2619 | Cr | 2013 |
| Zr | 3250 | Nb | 2470 | Mo | 2223 |
| Hf | 3660 | Ta | 3360 | W | 873 (decompose) |

### 1.4.5 Composition and stoichiometry

$MC_x$ is the general configuration of carbides where x can't be greater than 1, whereas, $MN_x$ is the general configuration of nitrides and here x can be greater than 1 also. It is seen that nitrogen's sub lattice is deficient for sub stoichiometric composition while metal lattice is deficient for hyper stoichiometric compositions.

### 1.4.6 Thermodynamic stability

The thermodynamic stability of parent metal atom of group IV-VI is less in comparison to the corresponding nitrides [26]. Moreover, the nitrides are highly catalytically active in comparison to their host metals. Thus, as we go from group IV-VI, the stability decreases because of the decrease in size of metal atom which leads to the difficulty in accommodation of nitrogen atom.

### 1.4.7 Heat of formation

The term heat of formation is the amount of heat released or absorbed when one mole of compound is formed. For nitrides, it is seen that as we move towards right in the periodic table from group IV-VI, heat of formation keeps on decreasing but among the group it is almost same.

### 1.4.8 Electronegativity

The difference in electronegativity of nitrogen and metal keeps on decreasing as we go from group IV to group VI. This is because there is qualitative relationship between electronegativity and ionic bonding, therefore, group IV metals forms strong ionic bonds in comparison to group VI.

## 1.5 Why molybdenum nitride?

Among the TMNs, the compound which has attracted the attention of scientist throughout the world is molybdenum nitride because of some unique properties exhibited by it. It includes many mechanical and electrical properties such as high wear strength and high chemical stability, corrosion resistance, high melting point, high thermal and electrical conductivity [27]. Most of the physical and chemical properties of molybdenum nitrides are similar to that of the other interstitial nitrides, but in addition to these it has some unique electronic, magnetic and catalytic properties [1]. Molybdenum forms a variety of nitrogen-containing compounds $MoN_x$ ($0 < x < 1$). Of all the phases, it mostly forms hexagonal (δ-MoN), fcc (γ-$Mo_2N$), body center tetragonal (β-$Mo_2N$) and tetragonal $Mo_{16}N_7$ phases [28]. Among these δ-MoN has excellent hardness (~30 GPa), which is almost comparable to that of diamond [15]. The β–$Mo_2N$ phase is stable at lower temperatures and it transforms to γ-$Mo_2N$ at higher temperatures [29]. Among all the Mo-nitride, the crystalline phase which dominates the most is γ-$Mo_2N$ in powder catalysis because of the fact that Mo atoms in γ-$Mo_2N$ are arranged in an fcc arrangement with $N_2$ atoms distributed randomly in half of the octahedral sites. This results in a Mo-Mo bond expansion which further induces a d-band contraction and at the Fermi level there's an increase of the density of state of Mo atoms, which shows that there is a similarity in electronic, magnetic and catalytic properties of the nitrides to the group VIII metals [30]. Molybdenum nitride is a potential candidate for high temperature

superconductors and diffusion barrier in microelectronic industry. It also shows some remarkable superconducting properties [31]. The recent advancements of $Mo_2N$ in industrial sector shows that it's being used in electrodes for charge storage thin film capacitors [30] and in high performance magnets [32]. The bulk synthesis of molybdenum nitride has found its usage in catalysis industry for a number of hydrogenation reactions such as hydrogenolysis and ammonia synthesis [18]. The catalytic properties of a material depends upon its surface area, morphology, which comes from the method of synthesis, time and temperature. To synthesize nano molybdenum nitride, having uniform size with high surface area at low temperature is still a big challenge. The most common methods used to synthesize high surface area γ-$Mo_2N$ catalysis are nitridation process of massive Mo (foil, powder) by $NH_3$ or molecular nitrogen, reduction of $MoO_3$ with $H_2$ and $N_2$ [32] mixture or $NH_3$ in a temperature programmed manner [33]. Some of the other methods may also include carbothermal nitridation of molybdenum oxide [15], reaction of $MoCl_5$ with urea [34] or molybdenum oxide with ammonium chloride ($NH_4Cl$) [35]. Thermal decomposition of few molybdate salts has also resulted in the yield of molybdenum nitride with exclusive properties. These molybdate salts include sodium molybdate ($Na_2MoO_4$) and (HMT)$(NH_4)_6Mo_7O_{24}$ where, HMT is hexamethylene tetra amine [36]. The nanopowders of γ-$Mo_2N$ have also been prepared via direct current arc discharge method [37]. However, recently high surface area molybdenum nitride has been synthesized via solid state metathesis reaction using $Ca_3N_2$ and $MoCl_5$ in the presence of $CaCl_2$ melt [38].

## 1.6 Phase diagram of molybdenum nitride

According to the phase diagram of Mo-N system as shown in Fig.1.3, it is seen that only few percent of nitrogen dissolves in the Mo metal and that to at very high temperature [39]. For Mo-N system, the most stable nitrides are $Mo_2N$ and MoN. At very high pressure, only MoN is formed. It can be understood from the phase diagram that $Mo_2N$ is only formed when high pressure along with high temperature is applied. At the temperature of 1860 $^oC$, only 1.08 at% N is dissolved in body centered Mo at about $6.7 \times 10^7$ Pa pressure. So, the corresponding content of nitrogen in γ-$Mo_2N$ is about 27 at %. The approximate melting temperature of $Mo_2N$ is around 2000 $^oC$. Furthermore, the $Mo_2N_{1\pm X}$ composition shows

that β-$Mo_2N$ (tetragonal) is a low temperature phase and γ-$Mo_2N$ (cubic) is a high temperature phase. All the three phases, β-$Mo_2N$, γ-$Mo_2N$ and α-Mo occur at the phase boundaries that are rich in molybdenum. The phase diagram also suggests that β-$Mo_2N$ possess stability above 800 $^oC$ with 28 at % composition of nitrogen.

The present work shows the synthesis of β-$Mo_2N$ at low temperature in an autoclave. The autoclave is high pressure vessel in which not only temperature but pressure also plays an important role for synthesis of $Mo_2N$. Here in this work, ammonium heptamolybdate (AHM) was taken as molybdenum source and Magnesium (Mg) as reducing agent. Along with AHM, sodium azide ($NaN_3$) was also taken which acted as a source of nitrogen. All these precursors were taken in particular amount and put in autoclave and heated in furnace at different temperatures ranging from 500 $^oC$ to 800 $^oC$ for varying time. The synthesized samples were then characterized by XRD, FE-SEM and TEM for structural and morphological studies.

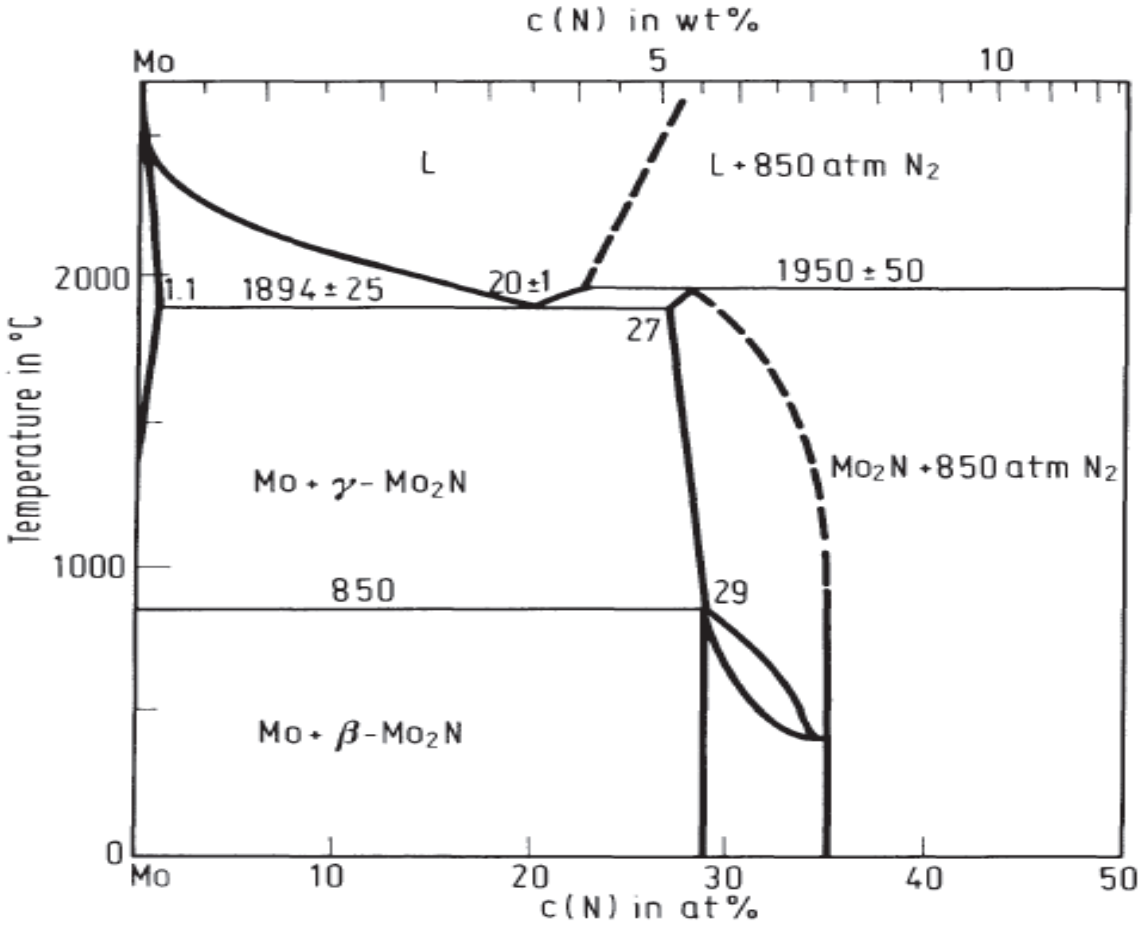


**Figure 1.3:** Phase diagram of molybdenum-nitrogen system [39].

## 1.7 References


[1] Greenwood N.N. & Earnshaw A., Nitrogen - chemistry of the elements (2nd edition), *Butterworth-Heinemann,* 406-472, (1997).

[2] Didziulis S.V., Butcher K.D. & Perry S.S., Small cluster models of the surface electronic structure and bonding properties of titanium carbide, vanadium carbide, and titanium nitride, *Inorg. Chem.,* **42,** 7766-7781, (2003).

[3] Pierson H.O., Handbook of refractory carbides and nitrides, *William Andrew publishing,* (1996).

[4] Ma J. & Du Y., A convenient thermal reduction-nitridation route to nanocrystalline molybdenum nitride ($Mo_2N$), *J. Alloys Compd.,* **463,** 196-199, (2007).

[5] Shy Y.M., Toth L.E. & Somasundaram R., Superconducting properties, electrical resistivities and structure of NbN thin films, *J. Appl. Phys.,* **44,** 5539-5545, (1973).

[6] Yamada T., Shimada M. & Koizumi M., Fabrication and characterization of titanium nitride by high pressure hot pressing, *J. Am. Ceram. Bull.,* **59,** 611-616, (1980).

[7] Pessall N., Gold E. & Johansen A., A study of superconductivity in interstitial compounds, *J. Phys. Chem. Solids.,* **29,** 374-378, (1968).

[8] Choi G., Choi D. & Thompson L.T., Preparation of molybdenum nitride thin films by N+ ion implantation, *J. Mater. Res.,* **7,** 374-378, (1992).

[9] Dover R.B., Hessen B., Werder D., Chen C.H. & Felder R.J., Investigation of ternary transition-metal nitride systems by reactive cosputtering, *Chem. Mater.,* **5,** 32-35, (1993).

[10] Furimsky E., Metal carbides and nitrides as potential catalysts for hydroprocessing, *Appl. Catal. A,* **240,** 1-28, (2003).

[11] Gregory D.H., Structural families in nitride chemistry, *J. Chem. Soc., Dalton Trans.,* 259-270, (1999).

[12] Seal S., Transition metal nitride functional coatings, *JOM-J. Miner. Met. Mater. Soc.,* **53,** 51-54, (2001).

[13] Langmir H.W. & McGrady G.S., Ternary nitrides for hydrogen storage: Li-B-N, Li-Al-N and Li-Ga-N systems, *J. Alloys Compd.,* **466,** 287-292, (2008).

[14] Hadjipanayis G.C., Nanophase hard magnets, *J. Magn. Mater.,* **200,** 373-391, (1999).

[15] S.T. Oyama, Chemistry of transition metal carbides and nitrides, *Blackie academic & professional*, London, (1996).

[16] Salamat A., Hector L., Kroll P. & McMillan P.F., Nitrogen-rich transition metal nitrides, *Coordination chem. Reviews,* **257,** 2063-2072, (2013).

[17] Zhang Y., Xia X., Shi F., Zhang J., Tu J. & Fan H.J., Transition metal carbides and nitrides in energy storage and conversion, *Adv.Sci.,* **3,** 1-28, (2016).

[18] Chuang J.C., Tu S.L & Chen M.C., Sputter-deposited Mo and reactively sputter-deposited Mo-N films as barriers layers against Cu diffusion, *Thin Solid Films,* **346,** 299-306, (1999).

[19] Wang S., Ge H., Sun S., Zhang J., Liu F., Wen X., Yu X., Wang L., Zhang Y., Xu H., Joerg C., Neuefeind., Qin Z., Chen C., Jin C., Li Y., He D. & Zhao Y., Zhao A., New molybdenum nitride catalyst with rhombohedral $MoS_2$ structure for hydrogenation applications, *J. Am. Chem. Soc.*, **137,** 4815-4822, (2015).

[20] Toth L.E., Transition metal carbides and nitrides, *Academic press London,* (1971).

[21] Hugh O.P., Handbook of refractory carbides and nitrides, *Noyes Publication, (1996).*

[22] Evans C., An introduction to crystal chemistry, *Cambridge Univ. Press,* (1964).

[23] Jauberteau I., Bessaudou A., Mayet R., Cornette J., Jauberteau J.L., Carles P. & Mejean T.M., Molybdenum nitride films: crystal structures, synthesis, mechanical, electrical and some other properties, *Coatings,* **5,** 656-687, (2015).

[24] Morkoc H., General properties of nitrides - handbook of nitride and semiconductors and devices, *Wiley-Vch,* **1,** (2008).

[25] Inumaru K., Baba K. & Yamanaka S., Synthesis and characterization of superconducting β-$Mo_2N$ crystalline phase on a Si substrate: an application of pulsed laser deposition to nitride chemistry, *Chem. Mater.*, **17,** 5935-5940, (2005).

[26] Ham D.J. & Lee J.S., Transition metal carbides and nitrides as electrode materials for low temperature fuel cells, *Energies,* 873-899, (2009).

[27] Wang S., Antonio D., Yu X., Zhang J., Cornelius A.L., He D. & Zhao Y., The hardest superconducting metal nitride, *Scientific Reports,* **5,** 1-7, (2015).

[28] Jehn H. & Ettmayer P., The molybdenum-nitrogen phase diagram, *J. Less-common Met., **58,*** 85-98, (1978).

[29] Papaconstantopoulos D.A., Pickett W.E., Klein B.M. & Boyer L.L., Electronic properties of transition metal nitrides: the group-V and group-VI nitrides VN, NbN, TaN, CrN, MoN, and WN, *Phys. Rev. B.*, **31,** 752-761, (1985).

[30] Reddy C.V.G., Manorama S.V. & Rao V.J., Effect of $Mo_2N$ on the gas-sensing characteristics of SnO2-based sensors, *J. Mater. Sci. lett.*, **18,** 673-676, (1999).

[31] Wang L., Tang K., Zhu Y., Li Q., Zhu B., Wang L., Si L. & Qian Y., Solid state synthesis of a new ternary nitride $MgMoN_2$ nanosheets and micromeshes, *J. Mater. Chem.*, **22,** 14559-14564, (2012).

[32] Lizana F.C., Quero S.G., Perret N., Minsker L.K. & Keane M.A., β-Molybdenum nitride: synthesis mechanism and catalytic response in the gas phase hydrogenation of p-chloronitrobenzene, *Catal. Sci. Technol.*, **1,** 794-801, (2011).

[33] Volpe L. & Boudart M., Compounds of molybdenum and tungsten with high specific surface area, *J. Solid State Chem.*, **59,** 332-347, (1985).

[34] Gomathi A., Sundaresan A. & Rao C.N.R., Nanoparticles of superconducting γ-$Mo_2N$ and δ-MoN, *J. of Solid State Chem.*, **180,** 291-295, (2007).

[35] Zhao X. & Range K.J., High pressure synthesis of molybdenum nitride MoN, *J. Alloys Compd.*, **296,** 72-74, (2000).

[36] Afanasiev P., New single source route to the molybdenum nitride $Mo_2N$, *Inorg. Chemistry*, **41,** 5317-5319, (2002).

[37] Shen L.H., Cui Q.L., Zhang J., Li X., Zhou Q. & Zou G.T., A new methof for preparation of nanocrystalline molybdenum nitride, *Chin. Phy. Lett.*, **22,** 3194-3194, (2015).

[38] Marchand R., Gouin X., Tessier F. & Laurent Y., S.T Oyama - New routes to molybdenum nitrides and oxynitrides: preparation and characterization of new phases, *Chapman & Hall*, 252-273, (1996).

[39] Jehn H. & Kurtz W., Gmelin Handbook of Inorganic Chemistry ($8^{th}$ Edition), *Springer-Verlag Berlin Heidelberg GmbH*, (1990).

## 2. Literature review

$Mo_2N$ is the most fascinating compound for scientist all around the world due to its high resistivity towards chemical attack at high temperatures, high hardness and catalytic activities similar to the conventional but costly metal catalysts (Pt, Pd, Rh etc.). The catalytic activity of nitrides is highly dependent on surface characteristics, which depends on synthesis route followed, as each process may lead to variations in surface composition and structure morphology. The conventional methods used for synthesis of molybdenum nitride exhibited large size of particle and low surface area. Scientists all over the globe are engaged in synthesis of nitrides at nano scale to extract enhanced catalytic properties. In comparison to work being carried out in developed countries like USA, Europe and Japan, the research in India in this field is at very slow rate. According to literature survey, till now not much work has been done on nano molybdenum nitride in India, whereas China has yielded maximum output in this fascinating and tantalizing area. The recent literature pertaining to the synthesis and application of $Mo_2N$ has been reviewed and presented here.

In 2000, **Janusz** [1] synthesized molybdenum and cobalt-molybdenum nitrides and investigated the activities of hydrodesulphurization (HDS) of thiophene. He also studied the structure and catalytic activity of Mo and Co-Mo nitride catalysts upon nitridation. The temperature programmed reduction method was adopted for the synthesis of Mo and Co-Mo nitrides. $MoO_3$ and Co-Mo oxides were taken as precursors for molybdenum and cobalt molybdenum nitrides respectively and ammonia as nitriding agent in a stainless steel reactor was used. All the oxides precursor were put into the reactor and were treated first in the air flow and then in ammonia flow. The temperature of apparatus was raised to 700 $^oC$ at the rate of 150 $^oC$/hr where it was kept for 1 hr and then cooled down to room temperature. XRD pattern showed that diffraction lines only attributed to the alumina support. The results predict enhancement of HDS activity by addition of cobalt which was almost the double of Molybdenum nitride.

In 2001, **Loughlin *et al.*** [2] synthesized cubic $Mo_2N$ from $MoCl_5$ and $Ca_3N_2$, where the former was taken as Mo source and the latter as $N_2$ source, under the pressure of 57 Kbar. Under these ambient conditions, the synthesized γ-$Mo_2N$ possessed high-surface area. 0.003 moles of $MoCl_5$ with $Ca_3N_5$ along with 3 mole of $NH_4Cl$ were taken and kept in

helium-filled dry box where all reactions took place, the ammonium chloride ($NH_4Cl$) acted as nitriding agent as well as heat sink for reactants. The samples were then washed with distilled water to eliminate any unreacted material. The BET of the prepared samples showed the surface area of 30 $m^2/g$.

In 2002, **Afanasiev *et al.*** [3] synthesized dispersed $Mo_2N$ particles possessing high surface area and lamellar morphology from the decomposition of $(HMT)_2(NH_4)_4Mo_7O_{24}$ salt, at different temperatures, ranging from 550-800 °C. Thermal decomposition of the homogeneous molecular precursor (which was a mixture of HMT (hexamethylenetetramine) and $(NH_4)_4Mo_7O_{24}$ (ammonium molybdate) yielded $Mo_2N$. Precursor was prepared by combining 3.5 g of $(NH_4)_4Mo_7O_{24}\cdot 4H_2O$ dissolved in 50 mL of distilled water and 6 g of HMT dissolved in 50 mL of water. These crystals were then heated at different temperatures (550, 650 and 800 $^oC$) in argon atmosphere and the product was then cooled to room temperature. The XRD results predict that the pure phase of $Mo_2N$ was obtained at 800 $^oC$ for 2 hrs. The surface area obtained was 158 $m^2/g$. SEM analysis of the sample showed thin sheets (lamellar structure) in the sub-micrometer range.

In 2003, **Kadono *et al.*** [4] synthesized intrazeolite molybdenum nitride (Mo/NaY) using chemical vapor deposition (CVD) method. The catalytic properties of prepared samples were studied and the results revealed that in comparison to sulfided Mo catalyst, molybdenum nitride was more stable to thiophene HDS activity. Hexacarbonyl molybdenum ($Mo(CO)_6$) was used as precursor for molybdenum and NaY zeolite was used as reference catalyst at 400 $^oC$. Ammonia gas ($NH_3$) was used for nitridation. Xanes spectra of the samples concluded that $Mo(CO)_6$ undergoes decomposition after the nitridation. Fourier transform analysis revealed the core shell size to be around 2 nm. The clusters of so formed molybdenum nitride were highly dispersed due to nitridation reaction at low temperatures.

In 2004, **Shi *et al.*** [5] synthesized cobalt molybdenum nitride and molybdenum nitride via the temperature programmed nitridation. Molybdenum trioxide ($MoO_3$) and cobalt molybdenum hydrate ($CoMoO_4.nH_2O$) were taken as precursors. Typically, ammonia gas was flowed in the reactor containing 2 g of oxide precursor. The temperature was

increased upto 700 $^{o}$C and maintained there for 2 hrs and then cooled down to room temperature under ammonia flow. These prepared catalysts were then used for the testing of NO reduction with $H_2$ and it was observed that Co-Mo nitride exhibited high stability and activity as compared to molybdenum nitride. XRD pattern revealed the formation of γ-$Mo_2N$ while SEM images revealed some of the particle having platelet structure while others have rod like structure. From BET analysis, the surface area of the particles were calculated to be 93 $m^2$/g.

In 2005, **Inumaru *et al.*** [6] synthesized molybdenum nitride (β-$Mo_2N$) with the help of pulse laser deposition (PLD) method on the Si substrates. For the synthesis of $Mo_2N$, $MoCl_5$ powder (0.2 g) in aluminum oxide ($Al_2O_3$) boat was placed in tubular furnace. The precursor was heated to 650 $^{o}$C at the heating rate of 10 $^{o}$C/min for 3 hrs under the flow of mixture of $N_2$ and $H_2$ gases. XRD results assured that the resultant product was β-$Mo_2N_{0.84}$ and the nitrogen content of this sample was determined with the help of elemental analyzer. It was also observed that below 5.2 K, molybdenum nitride β- $Mo_2N$ behaved as a superconductor.

In 2005, **Cai *et al***. [7] synthesized the $Mo_2N$ nanocrystals effectively via a liquid–solid metathesis reaction route. The reaction took place in stainless steel autoclave between the temperature ranges of 450-550 $^{o}$C for 12 hrs. $MoCl_5$ and sodium azide ($NaN_3$) were used as the source of molybdenum and nitrogen respectively. The synthesized product was then cleaned with dilute absolute ethanolic HCl and distilled water many times so as to remove any kind of impurities present. The obtained samples were then examined by XRD, TEM and XPS. XRD of the sample confirmed the formation of t-$Mo_2N$, while the TEM images showed the rod-like structures of the synthesized nanoparticles with varying lengths from 150-200 nm. The morphology and size of synthesized powders was affected by the change in temperature as the rod like structures became more visible with increase in temperature.

In 2006, **Panda *et al.*** [8] synthesized high surface area γ-$Mo_2N$ using the process of nitridation of oxide precursors. $MoO_3$, $H_2MoO_5$ (monoperoxomolybdic acid) and its hydrated form $H_2MoO_5.H_2O$ were taken as oxides precursors along with ammonia at 625 $^{o}$C. For the synthesis, 2 g of $MoO_3$ as a precursor was taken and then dissolved in $H_2O_2$

solution. The precipitates so obtained were then nitrided in tubular quartz reactor in an ammonia gas stream. The temperature was varied from 500 $^{o}$C to 700 $^{o}$C and then the samples were cooled down to room temperature. It was seen that on using different oxide precursors, nitrides of different phase composition and different specific surface areas were obtained. XRD analysis showed minor quantities of $MoO_2$ in many of the synthesized samples. Specific surface area of the particles were found to be 158.4 $m^2/g$ for γ -$Mo_2N$ samples when $H_2MoO_5 \cdot H_2O$ was used as precursor. Furthermore, the high value of surface area corresponds to an average particle diameter of 4 nm, which suggests that nanocrystals are cubic in nature.

In 2007, **Ma *et al.*** [9] synthesized molybdenum nitride (γ-$Mo_2N$) by the thermal reduction-nitridation reaction of anhydrous molybdenum pentachloride (1.639 g) as molybdenum source with ammonium chloride (0.214 g) as nitrogen source with metallic sodium (1.012 g) in a stainless steel autoclave at 550 $^{o}$C for 10 hrs sealed in the argon atmosphere. The final product obtained was then dried at 60 $^{o}$C in vacuum for 12 hrs. XRD results showed that the synthesized sample had cubic $Mo_2N$ structure, with a cell constant $a$ = 4.161 nm. The scanning electron microscopy (SEM) analysis of the powdered sample depicted that the average size of these particles was about 30 nm.

In 2007, **Chaudhuri *et al.*** [10] examined the size and structure of nanoparticles of molybdenum nitride, (prepared via direct current arc discharge method). The HR-TEM (high-resolution transmission electron microscopy) results predict that the particles were clustered together having average particle size between 3 and 5 nm. Along with the two prominent phases of molybdenum nitride i.e., γ-$Mo_2N$ (fcc) and δ-MoN (hexagonal), the molybdenum bcc phase was also present which might have been formed due to inadequate supply of $N_2$ or slow reaction rate. The γ-$Mo_2N$ and δ-MoN phases existed due to temperature gradient in reaction chamber where δ-MoN was formed at higher temperature (850 °C) and γ-$Mo_2N$ at lower temperature (500 to 700 °C).

In 2008, **Giordano *et al.*** [11] for the very first time obtained metal carbides and nitrides using urea as C and $N_2$ source, respectively. In first step $MoCl_5$ and $WCl_4$ were mixed with alcohol and a specific quantity of urea to form a polymer-like, glassy phase, which act as the starting product for other reactions. They found that it was feasible to synthesize

both carbides and nitrides of either molybdenum or tungsten by simply varying the metal precursor to urea molar ratio by heating this glassy phase. Urea played the role of both nitrogen and carbon source as well as stabilizing agent. It was found that molybdenum and tungsten nitride and carbides prepared by this method were pure and highly crystalline. Sizes estimated by Wide-angle X-ray scattering (WAXS) were in the range of 20 nm in diameter for Mo nitrides. The specific surface area was found lying between 10 and 80 $m^2/g$, depending on the initial ratio of metal precursor to urea.

In 2009, **Mazumdar *et al***. [12] synthesized porous nitride materials by using non-oxide sol gel method. The process involved the preparation of a colloidal solution of solid particles (sol) linked to immobilize the solvent to a point where the bulk shape gets stabilized (gel). Nano crystalline δ-MoN and γ-$Mo_2N$ with particle size of the range 10-30 nm were synthesized by heating nitride-tris (neopentyl) molybdenum, or bis (imido) derivative in $NH_3$ to 700 ºC. The carbon content of the product was lowered from 2 to 0.1% by heating upto 200 ºC. Replacing $NH_3$ with nitrogen in temperature range 500-700 ºC results in formation of nitrogen deficient $Mo_2N$. The product phase also showed the presence of higher carbon content which suggests the removal of carbon by formation of hydrocarbons was not complete at 500 ºC in $NH_3$ flow. $Mo_2N$ nano crystals of diameter ranging from 2-3 nm were obtained from complex compound $Mo(N^tBu)_2(Ph_2pz)_2$, when heated at 800 ºC under nitrogen flow .

In 2010, **Lizana *et al.*** [13] synthesized β-$Mo_2N$ from $MoO_3$ in $N_2/H_2$ by stepwise reduction of $MoO_3$ to $MoO_2$ and then finally to Mo. The obtained phase lead to the formation of β-$Mo_2N$ on further nitridation. $MoO_3$ was used as a precursor and 0.15 g of it was loaded in U-shaped quartz cell and then heated in 15 % v/v $N_2/H_2$ at 5 ºC/min to 660 ºC for 3 hrs. A steam was passed through liquid $N_2$ and with the help of thermal conductivity detector (TCD) the changes in composition of $N_2$ were recorded. The transformation from Mo to β-$Mo_2N$ was non topotactic morphology with disruption in the platelet structure which is confirmed by SEM analysis with increase in surface area from 1-17 $m^2/g$. The synthesized powder acts as a low cost catalyst for production of aromatic amines in chemical industry.

In 2011, **Wu *et al.*** [14] synthesized $Mo_2N$ and $W_2N$ flexible counter electrodes (CEs) on Titanium (Ti) nano sheets via magnetron sputtering system under Ar and $N_2$ as sputter and reactive gas respectively. The as prepared materials showed excellent catalytic activities for triiodide to iodide reduction. They also act as efficient counter electrodes in dye-sensitized solar cell (DSC). XRD confirms the presence of γ-$Mo_2N$ phase. Sputtered films of $Mo_2N$ and $W_2N$ films had thickness of 650 nm and 500 nm respectively which can be visualized from the SEM images. The development of low cost $Mo_2N$ and $W_2N$ CEs are promising potential substitutes for expensive platinum (Pt). The work demonstrates the utilization of DSCs for industries.

In 2012, **Qian *et al.*** [15] synthesized a new ternary nitride ($MgMoN_2$) via solid state synthesis using sodium azide ($NaN_3$) as nitrogen source and Molybdenum trioxide ($MoO_3$) as molybdenum precursor. Magnesium was used as reducing agent. The process took place in a stainless steel autoclave at 700 $^oC$. For synthesis of molybdenum nitride nanocrystals, 1.43 g of $MoO_3$, 4 g of $NaN_3$ and 0.3 g of magnesium were mixed well in agate mortar and then transferred to autoclave for heating which was maintained at 700 $^oC$ for 10 hrs. The final product after cooling to room temperature was washed several times with HCl and ethanol to remove any byproduct formed. $MgMoN_2$ micromesh was also obtained by reacting $MoO_3$ and $NaN_3$ in different quantities in the presence of magnesium. The replacement of $MoO_3$ with any other molybdenum source resulted in micromeshes of different pore sizes. The characterization of obtained products showed that as-prepared $Mo_2N$ exhibited cubic structure and $MgMoN_2$ crystal comprised of alternate layers of $MgN_6$ octahedral and $MoN_6$ trigonal prisms. The TEM and FE-SEM analysis showed that $MgMoN_2$ nanosheets possessed the diameter of few micrometers and thickness of 30 nm. The selected-area electron diffraction (SAED) depicted that $MgMoN_2$ is made up of single crystalline micromeshes. The as prepared materials act as catalyst for chemical filteration in chemical industries.

In 2012, **Xiaodong *et al.*** [16] utilized ion-beam-assisted-deposition (IBAD) method for the synthesis of molybdenum nitride by means of magnetron sputtering method. A pure target of molybdenum was used for deposition in the presence of Ar and $N_2$ atmosphere. The MoN coatings were synthesized on Si-wafer substrate and during deposition nitrogen

ion beam was bombarded. The argon ion beam was used to sputter and then etch the sample before deposition and Si wafer single crystal was used as the substrate. During the synthesis, the base pressure flow variation was from $1\times10^{-3}$ Pa to 0.2 Pa with the total mass flow of argon and nitrogen as 30 sccm. It was observed that with the increase of partial pressure ratio of nitrogen to argon, change in phase from $Mo_2N$ to MoN observed was confirmed by XRD. The further investigations revealed that the high bombarding energy, in addition to high $N_2$ partial pressure was also necessary for the formation of single phase MoN. Moreover, the coating of single phase MoN is better than $Mo_2N$ thereby showing enhancement in both mechanical properties and oxidation resistance.

In 2013, **Lee *et al.*** [17] prepared $Mo_3N_2$ nanowires by using topotactic reaction. The single crystalline nanowires of molybdenum oxide ($MoO_3$) were used as starting material for the synthesis of single crystalline mesoporous nanowires of molybdenum nitride (meso-$Mo_3N_2$-NWs). It was observed by the nitrogen sorption measurement that the synthesized nitride possessed the specific area and the pore size of 45 $m^2/g$ and 4.6 nm respectively. Due to this increase in the mesoporous structure and specific surface area, the $Mo_3N_2$-NWs exhibited superior charging and discharging properties and specific capacitance in comparison to the properties shown by $Mo_3N_2$, prepared by the commercial nitridation process of $MoO_3$.

In 2013, **Zhang *et al.*** [18] synthesized molybdenum nitride (size ~50 nm) by hydrothermal method succeeded by ammonia annealing. The synthesized MoN samples showed considerable amount of electro catalytic activity toward oxygen reduction reaction (ORR) in case of nonaqueous electrolytes. MoN/N-C particles were used as cathode catalyst for Li-$O_2$ batteries where tetra dimethyl ether was used as the electrolyte. The MoN nanospheres were prepared by reduction of $MoO_2$ nano spheres in ammonia atmosphere with cyanamide ($CH_2N_2$) as the structure confinement agent. It was demonstrated that life span of Li-$O_2$ batteries was enhanced using MoN/N-C nano spheres as the cathode catalyst. HR-TEM images revealed well textured and single crystalline nanospheres and their porosity was obtained by determining the $N_2$ adsorption-desorption isotherms. These kinds of transition metal nitrides could reduce over potentials during the charging-discharging processes thereby indicating a promising

candidate for a cathode catalyst in Li-$O_2$ battery applications. The synergetic effects of MoN/N-C nano spheres delivered abundant surface active sites and excellent electro-catalytic activity.

In 2014, **Park *et al.*** [19] synthesized mesoporous molybdenum nitride nanobelts for the lithium-ion batteries as an anode materials using template free synthesis method. These prepared meso-$Mo_2N$ nanobelts showed the face centered cubic 1-dimensional structure. The synthesis of this molybdenum nitride nanobelts was done using molybdenum trioxide and ammonium molybdate as the precursors dissolved in $HNO_3$ and heated in autoclave for 4 hrs at 160 $^oC$. The resulting molybdenum oxide powder was then heated at 700 $^oC$ under the $NH_3$ flow and finally molybdenum nitride nanobelts were formed. The structural analysis done using TEM, SEM and HR-TEM revealed that meso-$Mo_2N$-NBs had the average length and width of 3.5 µm and 550 µm respectively and the pore size of 4 nm. The results also predicted high surface area ratio of as prepared nanobelts as compared to the commercially prepared $Mo_2N$ nanoparticles. The as-prepared meso-$Mo_2N$ nanobelts showed high specific capacity and outstanding rate of cycling performance due to high diffusion coefficient and low transport resistance.

In 2015, **Xiao *et al.*** [20] synthesized titanium molybdenum nitride ($Ti_{0.8}Mo_{0.2}N$) by one-pot solvothermal process followed by thermal treatment under ammonia at 750 °C, which was further coated with Platinum nanoparticles to catalyze the oxidation of methanol. An aqueous solution containing 1.09 g $MoCl_5$ and 3.03 g $TiCl_4$ precursors were prepared and stirred for 30 min. The prepared solution was then poured inside an autoclave and kept at 150 °C for 3 hrs. The precipitates were cooled down to the room temperature, followed by their washing with distilled water and then drying in air at 80 °C overnight. Precursors were then placed in the tubular furnace, annealed at 750 °C under the flow of ammonia gas for almost 2 hrs with increasing heating rate. MoN nanoparticles were prepared by taking $MoCl_5$ as the only precursor. XRD structure revealed that fcc $Ti_{0.8}Mo_{0.2}N$ was formed. HR-TEM images showed a dense solid comprised of nanoparticles with lattice fringes calculated to be 0.252 nm. The study showed that Pt/$Ti_{0.8}Mo_{0.2}N$ have a much higher catalytic activity and durability than conventionally prepared Pt/C

electrocatalysts. This enhancement in properties of $Pt/Ti_{0.8}Mo_{0.2}N$ catalysts is due to the synergistic effect introduced by the Mo doping.

In 2015, **Liang *et al.*** [21] synthesized $Mo_2C$ and $Mo_2N$ nanoparticles via 'urea glass' route for the hydrogen evolution reaction (HER). With the simple variation in the molar ratio of the urea to metal precursor, α-$Mo_2C$ and γ-$Mo_2N$ of pure phase, crystalline, and monodisperse in size, were obtained. For the synthesis of molybdenum nitride or carbide, molybdenum orthoesters were prepared using the solid metal precursor $MoCl_5$ dissolved in ethanol. Solid urea was then added to the alcoholic solution in different quantities to get the required urea/metal precursor molar ratio (R). The mixture was then stirred to completely dissolve the urea, which indicates the formation of coordination polymers and soluble complexes. Then these precursors were kept in crucibles and heated for 3 hrs under the flow of $N_2$ gas at 800 $^oC$. After this the silvery black powders were obtained indicating the formation of carbides and nitrides. Further examination of prepared samples revealed that $Mo_2N$ showed extraordinary catalytic activity towards the hydrogen evolution reaction. XRD results confirms the presence of γ-$Mo_2N$ phase while the particle size was calculated by the Scherrer method in the range of 11-16 nm. The BET surface areas of the $Mo_2C$ and $Mo_2N$ catalysts were found to be 9.1 and 9.8 $m^2 g^{-1}$, respectively.

In 2016, **Liu *et al.*** [22] synthesized the single crystal like and highly porous $Mo_2N$ nanobelts by topotactic chemical transformation from single crystal $MoO_3$ nanobelts. The prepared powders are promising substitute to expensive platinum catalysts for development of fuel cells. The ultrafine Nano porous $Mo_2N$ nanobelts of high density were produced by solid state reaction. 2 g of $MoO_3$ powder was mixed with 20 mL of $H_2O_2$ and stirred overnight on magnetic stirrer until it becomes yellow in color, after this 20 mL of $H_2O$ was added and then the whole solution was transferred to 120 mL Teflon liner which was put inside an autoclave and kept in oven at 190 $^oC$ for 12 hrs. The final product was washed several times with both ethanol and distilled water and then dried at 80 $^oC$ for 12 hrs in vacuum. It was seen that $Mo_2N$ nanobelts showed the high electrocatalytic activity in alkaline electrolyte and emerges out to be the most capable Pt-free cathodic electrocatalysts in fuel cells. The synthesized nanobelts of molybdenum

nitride also showed high specific capacitance (160 F/g), high cycling stability and ability to act as supercapacitors electrode material.

In 2017, **Mishra *et al.*** [23] successfully synthesized the nano-structured and porous γ-$Mo_2N$ and γ-$Co_{0.25}Mo_{1.75}N$ materials by the metal ions reaction. Both the prepared γ-$Mo_2N$ and γ-$Co_{0.25}Mo_{1.75}N$ materials exhibited fcc crystal structure. For the synthesis of γ-$Mo_2N$, firstly, the oxide precursor was prepared using Ammonium heptamolybdate tetrahydrate $(NH_4)_6Mo_7O_{24}.4H_2O$ dissolved in distilled water. After that when complete dissolution takes place then hydrazine hydrate solution was added at room temperature. The solution so obtained was then refluxed at 70˚C for 30 min in air. The precipitates were then heated under $N_2$ flow at 700 ºC and the resulting precipitates were then characterized using SEM, BET, TEM, XRD and HR-TEM. TEM and XRD studies showed nanocrystals of γ-$Mo_2N$ and γ-$Co_{0.25}Mo_{1.75}N$ nitrides having particle sizes of 5 and 12 nm and crystallite sizes of 6 and 11 nm, respectively which is confirmed from TEM images, while, HR-TEM study showed that as synthesized samples possessed lattice stacking and porous structures. The BET results revealed that the surface area for γ-$Mo_2N$ and γ-$Co_{0.25}Mo_{1.75}N$ nitride material is 53 and 12 $m^2/g$, respectively. Also the M vs H plots of γ-$Co_{0.25}Mo_{1.75}N$ and γ-$Mo_2N$ depict weak ferromagnetism possessing coercivities values of 2838 and 296 Oe, respectively.

In 2017, **Mosavati *et al.*** [24] in their work, synthesized $Mo_2N$, VN, WN and studied the surface composition and electrochemical performance of cathodes electrodes for Lithium sulfur batteries. Furthermore, they also investigated the lipopolysaccharide (LPS) conversion reactions mechanism of these transition metal nitrides. The capacities of WN, VN and $Mo_2N$ were found to be 697 mAH $g^{-1}$, 573 mAH $g^{-1}$ and 264 mAH $g^{-1}$ respectively. The synthesis of molybdenum nitride took place inside autoclave at 160 ºC for 3 hrs after the 1 hr stirring of ammonium molybdate tetrahydrate in 5M $HNO_3$ at room temperature. The molybdenum oxide powders obtained were then washed with ethanol and dried in oven and then heated under $NH_3$ flow at 700ºC and then cooled at room temperature. The resulting molybdenum nitride powders possessed the mesoporous nano-rod shaped morphology with average particle diameter as 850 nm and length of 75 nm. The crystallite structure and surface area was found to be fcc and 10.2 $m^2/g$ respectively.

In 2017, **Podila *et al.*** [25] synthesized molybdenum nitride catalyst using ammonium hepta molybdate ($(NH_4)_6Mo_7O_{24}.4H_2O$) and citric acid. The precursor made up of citric acid and molybdenum salt solution was aged in water bath for 24 hrs and then dried in oven at 110 $^oC$ for 24 hrs. The resulting material was then calcined in furnace at 500 $^oC$ for 5 hrs. They also examined the hydrogen production from the decomposition of ammonia using sequence of unsupported high surface area cobalt promoted molybdenum nitride (Co-$Mo_2N$) and molybdenum nitride ($Mo_2N$) catalysts formulated with citric acid (CA), which acts as a chelating agent. The effect of CA/Mo ratio on structure and catalytic activity was also studied. To study surface, surface area, surface chemistry, morphology, crystal structure and elemental composition, the sample were characterized by BET, XPS, SEM, TEM, XRD and EDS respectively. SEM and TEM images revealed the pseudomorphous morphology of the γ-$Mo_2N$ indicating that molar ratio has a great impact on formation of particles. The further investigation on these catalysts revealed their exceptional performance in production of $H_2$.

In 2017, **Xiaojuan *et al.*** [26] synthesized monometallic molybdenum nitride $Mo_2N$ and the bimetallic molybdenum nitrides $Ni_3Mo_3N$ and $Co_3Mo_3N$. It was found that these materials were catalytically active in the dry reforming of methane (DRM) reaction above 550 °C. In comparison to $Mo_2N$, $Co_3Mo_3N$ and $Ni_3Mo_3N$ had superior properties like enhanced catalytic activity, stability and resistant to oxidation. Especially, $Co_3Mo_3N$ exhibited highest activity and stability among all the three nitrides, due to three factors; first being the synergistic effect between heterometals, secondly almost equal adsorption capacity and thirdly due to the consumption rates of reactants. The $MoO_3$ precursor was prepared by calcination of $(NH_4)_6Mo_7O_{24}$ (AHM) at 400 °C for 2 hrs in dry air. After drying at 100 °C overnight, the obtained solid products were calcined at 400 °C in dry air. $MoO_3$ precursor was then placed on a porcelain combustion boat and nitrided in tube furnace by a temperature-programmed reaction with ammonia which was programmed to heat the sample in three stages: (1) The temperature was raised from ambient to 300 °C at a rate of 5 °C/min, (2) then to 700 °C at 1 °C/min, (3) Finally, the furnace was kept at 700 °C for 3 hrs. At the end of program, ammonia was allowed to flow and the product was quenched. BET analysis showed the size of $Mo_2N$ to be around 23.24 $m^2/g$ with the

particle range between 10-20 nm. Also, the active adsorption centers over $Mo_2N$ at high temperature were relatively rare which is unfavorable for the DRM reaction. However,

the $CH_4$ consumption for $Mo_2N$ was negligible, but the consumption peaks of $CO_2$ appeared both at low and high temperature, indicating that the $Mo_2N$ was very sensitive to CO and partial consumption is related to the surface oxidation. The results of their experiment suggested that the low-cost $Co_3Mo_3N$ can be a promising candidate for DRM.

## 2.1 References


[1] Janusz T., Effect of synthesis conditions on the hydrodesulphurization and hydrodenitrogenation activities of alumina supported Mo and CoMo nitrides, A*pplied Catal.,* **197,** 289-293, (2000).

[2] O'Loughlin J., Wallace C.H., Knox M.S. & Kaner R.B., Rapid Solid-State Synthesis of tantalum, chromium, and molybdenum nitrides, *Inorg. Chem*., **40,** 2240-2245, (2001).

[3] Afanasiev P., New single source route to the molybdenum nitride $Mo_2N$, *Inorg. Chemistry.*, **41**, 5317-5319, (2002).

[4] Kadono T., Kubota T. & Okamoto Y., Hydrodesulphurization over intrazeolite molybdenum nitride clusters prepared by using hexacarbonyl molybdenum as a precursor, *Catalysis Today*, **87,** 107-115, (2003).

[5] Shi C., Zhu A.M., Yang X.F. & Au C.T., NO reduction with hydrogen over cobalt molybdenum nitride and molybdenum nitride: a comparison study, *Catalysis Letters*, **97,** 9-16, (2004).

[6] Inumaru K., Baba K. & Yamanaka S., synthesis and characterization of superconducting-$Mo_2N$ crystalline phase on a Si substrate: an application of pulsed laser deposition to nitride chemistry, *Chem. Mater.*, **17**, 5935-5940, (2005).

[7] Cai P., Yang Z., Wang C., Gu Y. & Qian Y., A simple approach to synthesize $Mo_2N$ nanocrystals, *Chem. Lett.*, **34,** 1360-1361,(2005).

[8] Panda R.N. & Kaskel S., Synthesis and characterization of high surface area molybdenum nitride, *J. mater. Sci.*, **41,** 2465-2470, (2006).

[9] Ma J. & Du Y., A convenient thermal reduction-nitridation route to nanocrystalline molybdenum nitride ($Mo_2N$), *J. Alloys Compd.*, **463,** 196-199, (2007).

[10] Chaudhuri J., Nyakiti L., Lee R., Ma Y., Li P., Cui Q.L. & Shen L.H., Molybdenum nitride nanoparticles - high-resolution transmission electron microscopy study, *Mater. Lett.*, **61,** 4763-4765, (2007).

[11] Giordano C., Erpen C., Yao W. & Antonietti M., Synthesis of Mo and W carbide and nitride nanoparticles via a simple 'urea glass' route, *Nano Lett.*, **8,** 4659-4663 (2008).

[12] Mazumder B. & Hector A. L. Solution phase preparative routes to nitride morphologies of interest in catalysis, *Top. Catal.,* **52,** 1472-1481, (2009).

[13] Lizana F., Quero S., Perret N., Minsker L. & Keane M.A., Beta-Molybdenum nitride: synthesis mechanism and catalytic response in the gas phase hydrogenation of p-chloronitrobenzene, *Catal. Sci. Technol.,* **1,** 794-801, (2010).

[14] Wu M., Zhang Q., Xiao J., Ma C., Lin X., Miao C., He Y., Gao Y., Hagfeldt A & Ma T., Two flexible counter electrodes based on molybdenum and tungsten nitrides for dye-sensitized solar cells, *J. Mater. Chem.,* **21,** 10761-10766, (2011).

[15] Zhu Y., Li Q., Mei T. & Qian Y., Solid state synthesis of nitride, carbide and boride nanocrystals in an autoclave, *J. Mater. Chem.,* **21,** 13756-13764, (2012).

[16] Zhu X., Yue D., Shang C., Fan M. & Hou B., Phase composition and tribological performance of molybdenum nitride coatings synthesized by IBAD, *Surf. Coatings Technol.,* **228,** 184-189, (2012).

[17] Lee K.H., Lee Y.W., Ko A.R., Cao G. & Park K.W., Single-crystalline mesoporous molybdenum nitride nanowires with improved electrochemical properties, *J. Am. Ceram. Soc.,* **96,** 37-39, (2013).

[18] Zhang K., Zhang L., Chen X., He X., Wang X., Dong S., Gu L., Liu Z., Huang C. & Cui G., Molybdenum nitride/n-doped carbon nanospheres for lithium-$O_2$ battery cathode electrocatalyst, *ACS Appl. Mater. Interfaces,* **5,** 3677-3682, (2013).

[19] Park H.C., Lee K.H., Lee Y.W., Kim S.J., Kim D.M., Kim M.C & Park K.Y., Mesoporous molybdenum nitride nanobelts as an anode with improved electrochemical properties in lithium ion batteries, *J. Power Sources,* **269,** 534-541, (2014).

[20] Xiao Y., Fu Z., Zhan G., Pan Z., Xiao C., Wu S., Chen C., Hu G. & Wei Z., Increasing Pt methanol oxidation reaction activity and durability with a titanium molybdenum nitride catalyst support, *J. Power Sources,* **273,** 33-40, (2015).

[21] Ma L., Ting L.R.L., Molinari V., Giordano C. & Yeo B.S., Efficient hydrogen evolution reaction catalyzed by molybdenum carbide and molybdenum nitride nanocatalysts synthesized via the urea glass route, *J. Mater. Chem.,* **3,** 8361-8368, (2015).

[22] Liu J., Huang K., Tang H.L. & Lei M., Porous and single-crystalline-like molybdenum nitride nanobelts as a non-noble electrocatalysts for alkaline fuel cells and electrode materials for supercapacitors, *International J. hydrogen energy,* **41,** 996-1001, (2016).

[23] Mishra P. P. & Panda R. N., Novel synthesis, characterization and magnetic properties of nano-structured γ-$Mo_2N$ and γ-$Co_{0.25}Mo_{1.75}N$ nitrides, *Mater. Res. Bull.*, **86,** 241-247, (2017).

[24] Mosavati N., Salley S.O. & Ng K.Y.S., Characterization and electrochemical activities of nanostructured transition metal nitrides as cathode materials for lithium sulfur batteries, *J. Power Sources,* **340,** 210-216, (2017).

[25] Podila S., Zaman S.F., Driss H., Alhamed Y.A., Zahrani A. & Petrov L.A., High performance of bulk $Mo_2N$ and $Co_3Mo_3N$ catalysts for hydrogen production from ammonia: Role of citric acid to Mo molar ratio in preparation of high surface area nitride catalysts, *Catal. Sci. Technol.*, **6**, 1496-1506, (2017).

[26] Fu X., Su H., Yin W., Huang Y. & Gu X., Bimetallic molybdenum nitride $Co_3Mo_3N$: a new promising catalyst for $CO_2$ reforming of methane, *Catal. Sci. Technol.*, **7,** 1671-1678, (2017).

# 3. Experimental

## 3.1 Materials

In this thesis, an attempt was made to synthesize the nanopowders of molybdenum nitride ($Mo_2N$) by reduction-nitridation route in a specially designed autoclave. Materials used for this purpose are ammonium heptamolybdate tetrahydrate (AHM) ($(NH_4)_6Mo_7O_{24}.4H_2O$), (*SDFC Ltd. extrapure*) as molybdenum source. Sodium azide ($NaN_3$ *99% LR, SDFC Ltd*.) is used as nitrogen source. Magnesium (Mg) powder (*SDFC Ltd.*) was used as a reducing agent. The detailed methodology for the synthesis of $Mo_2N$ is given below:

## 3.2 Methodology

All the samples were synthesized in an autoclave (stainless steel-high grade). An initial mixture of AHM (2.87 g) and Mg (2.00 g), prepared by mixing them in agate-mortar, was put into the autoclave of 30 mL capacity. Moreover, $NaN_3$ (1.00 g) was added to enhance the process of nitridation. The reaction process was carried at various holding times (1, 10, 12, 15, 20 hrs) at different temperatures (500, 600, 700, 800 °C) at a constant heating rate of 5 °C/min in a furnace. The autoclave was heated from room temperature to desired temperature for defined duration. After that the autoclave was allowed to cool to room temperature inside the furnace itself. Effect of temperature and time was studied to get single phase $Mo_2N$. The variation in quantities of precursor and nitrogen source was done so as to obtain the pure phase of β-$Mo_2N$. The synthesized powder obtained after heating the autoclave to particular temperature and time was washed several times with dilute solution of (1:1) HCl so as to remove undesired impurities. The powder was then subjected to washing for several times with distilled water. The obtained powder is then dried in an oven at 120 °C for 24 hrs. Fig.3.1 shows the schematic representation of synthesis process and Table 3.1 shows the experimental conditions with variation in different synthesis conditions:

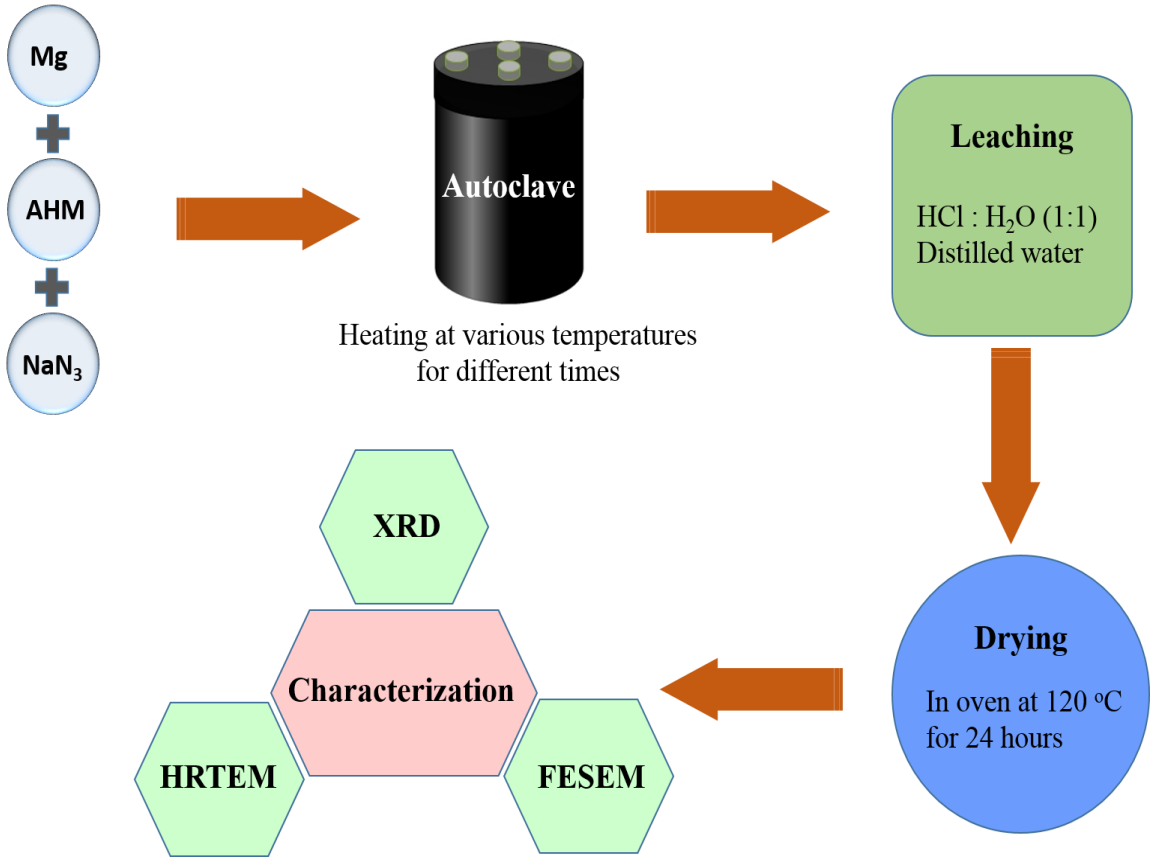


**Figure 3.1.** Schematic representation of $Mo_2N$ synthesis.

**Table 3.1.** Details of the synthesis conditions of $Mo_2N$.

| Sample Id | AHM (g) | Mg (g) | $NaN_3$ (g) | Temperature (°C) | Holding time (hrs) |
|---|---|---|---|---|---|
| M1 | 3 | - | - | - | - |
| M2 | 3 | - | - | 800 | 1 |
| M3 | 2.8792 | 2.0025 | - | 800 | 1 |
| M5 | 2.8792 | 2.0032 | - | 500 | 10 |
| M6 | 2.8873 | 2.0046 | - | 600 | 10 |
| M7 | 2.8790 | 2.0008 | - | 700 | 10 |
| M8 | 2.8848 | 2.0056 | - | 800 | 10 |
| M9 | 2.8797 | 2.0002 | 1.0009 | 600 | 10 |
| M10 | 2.8792 | 2.0002 | 1.0007 | 700 | 10 |
| M11 | 2.8798 | 2.0031 | 1.0093 | 600 | 15 |

| | | | | | |
|---|---|---|---|---|---|
| M12 | 2.8792 | 2.0009 | 1.0003 | 600 | 20 |
| M13 | 2.8795 | 2.0021 | 1.0094 | 700 | 12 |
| M14 | 2.8789 | 2.0007 | 1.5007 | 700 | 12 |
| M15 | 2.8785 | 2.0008 | 2.0008 | 700 | 12 |
| M16 | 1.2357 | 2.0005 | 2.0002 | 700 | 12 |
| M17 | 2.8788 | 2.0018 | 2.5005 | 700 | 12 |
| M18 | 2.8788 | 2.0009 | 3.0072 | 700 | 12 |

## 3.3 Characterizations

### 3.3.1 X-ray diffraction (XRD)

A non-destructive technique called X-ray diffraction is used to determine purity, crystal structure, composition and properties [1] of sample formed. When an incident beam of X-rays hit the atomic crystal planes it undergoes interference with one another as they come out of the crystal. This phenomenon is called X-ray diffraction or XRD. The position of these planes are given by Bragg's law (1912),

$$\boldsymbol{2dsin\theta = n\lambda} \qquad \text{(ii)}$$

where, d = inter-planar distance (in nm), λ = wavelength of incident X-ray (in nm), θ = diffraction or Bragg's angle (in degrees) and n = order of the diffraction. The samples were characterized by using the *PANALYTICAL X'PERT PRO* XRD diffractometer having Cu-Kα radiation with inbuilt Ni filter and λ = 1.5418 Å. The applied voltage was 45 kV. The XRD data was collected from $20° \leq 2\theta \leq 80°$ with step size of 0.0131°. All the peaks were matched and analyzed with the diffraction cards provided by International Centre for Diffraction Data (ICDD) using *X'pert HighScore plus*. Line profile analysis of XRD data allows to determine the size and strain of the product. The crystallite size was determined by the commonly used Scherrer method.

### 3.3.2 Field emission scanning electron microscopy (FE-SEM)

A microscopic technique that uses an electron beam for sample analysis is scanning electron microscope (SEM) [2]. In SEM, the sample is scanned by the electromagnetic fields generated with the help of acceleration of electrons between the energy ranges of few hundred eV to 40 keV. SEM can be used at high magnification upto few hundred

nanometers. EDS attached to it can give composition of the sample where back scattered electrons are used. In field emission scanning electron microscopy (FE-SEM), the field emission gun is the electron source, which improves the image quality. For FE-SEM analysis, samples M15 and M16 were analyzed in powder form by placing them on C tape. Then, platinum (Pt) coating was done on the samples placed on C tape so as to make the surface conducting. The samples were analyzed with *HITACHI - SU8010* operating at the voltage of 15 kV.

### 3.3.3 High-resolution transmission electron microscopy (HR-TEM)

HR-TEM is an imaging mode that helps to examine the properties of materials on the atomic scale. In this microscopy, the electron beam is transmitted through the ultra-thin sample [3]. The magnified image of both, scattered and un-scattered electrons, is obtained from it and focused on an imaging device. This image formed is then detected by a charge coupled device (CCD). HR-TEM is useful in obtaining the atomic spacing, structural defects, crystal interfaces and the individual grain size. Samples M15 and M16 were first dispersed in ethanol and were placed for approximately 30 mins in sonicator. A drop of this liquid was deposited on the copper grid and dried at room temperature. The samples were analyzed with *JEOL 2100* operating at 200 kV.

## 3.4 References

[1] Bunaiciu A.A., Udristioiu E.G. & Enien H.Y., X-Ray Diffraction: instrumentation & applications, *Critical review in analytical chem.*, **45,** 289-299, (2015).

[2] Carter M. & Shieh J., Microscopy - guide to research technique in neuroscience, *Academic press,* **2,** 117-144, (2015).

[3] Joshi M., Bhattacharya A. & Ali S.W., Characterization techniques for nanotechnology applications in textiles, *Indian J. of fiber & textile research,* **33,** 304-317, (2008).

# 4. Results and Discussion

The present work emphasizes the effect of reaction temperature (500 to 800 $^{o}$C) and reaction time on the synthesis of nano molybdenum nitride. At first ammonium heptamolybdate tetrahydrate (AHM) $(NH_4)_6Mo_7O_{24}.4H_2O$ was used as molybdenum precursor and nitrogen source. But the decomposition of AHM shows the formation of $MoO_3$, $MoO_2$, Mo and a little of $Mo_2N$ at different temperatures and time conditions. To enhance the nitridation process, $NaN_3$ was used as an additional nitrogen source along with AHM to obtain single phase $Mo_2N$ at later stages. The synthesized nanopowders were characterized by X-ray diffraction (XRD), Field emission scanning electron microscope (FE-SEM) and high resolution transmission electron microscope (HR-TEM).

## 4.1 XRD (X-ray diffraction)

To identify the different compounds and phases present in as prepared samples, the XRD analysis was done by *X'Pert HighScore Plus* software for different ICDD (International Centre for Diffraction Data) reference patterns. The ICDD reference cards used for different phases are given in Table 4.1.

**Table 4.1:** List of ICDD reference cards used in analysis.

| S.no | ICDD card no. | Compound |
|---|---|---|
| 1 | 01-075-1150 | t-$Mo_2N$ |
| 2 | 01-089-5023 | Mo |
| 3 | 00-025-1366 | c-$Mo_2N$ |
| 4 | 00-027-1013 | AHM |
| 5 | 00-032-0671 | $MoO_2$ |
| 6 | 00-023-1256 | $Mo_{16}N_7$ |
| 7 | 00-025-1367 | MoN |
| 8 | 01-080-0757 | $(NH_4)_2Mo_4O_{13}$ |
| 9 | 03-065-4278 | $Mo_3N_2$ |
| 10 | 00-051-1326 | $Mo_5N_6$ |
| 11 | 03-065-6236 | $Mo_2N_{0.76}$ |

| | | |
|---|---|---|
| 12 | 01-089-1554 | $MoO_3$ |
| 13 | 00-036-0031 | $(NH_4)_2Mo_3O_{10}$ |

## 4.1 (A) Effect of reaction temperature on the synthesis of nano molybdenum nitride

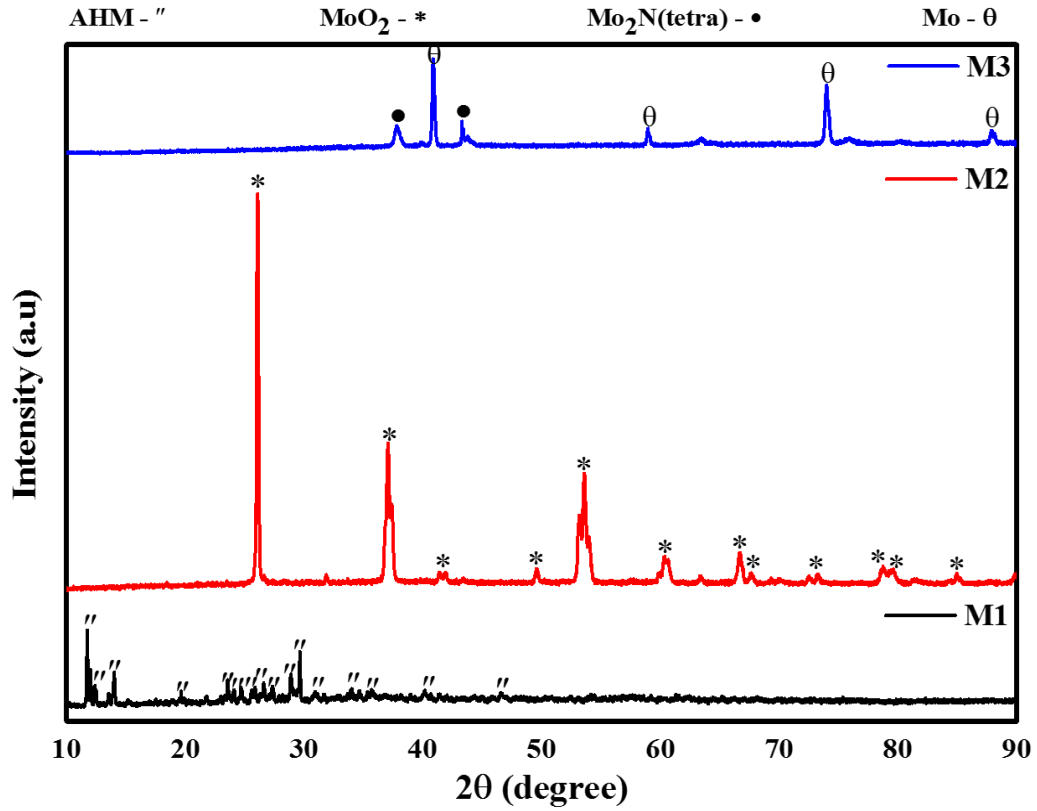


**Figure 4.1:** XRD pattern of pure AHM (M1), thermal decomposition of precursor AHM in the absence (M2) and in the presence (M3) of Mg at 800 $^oC$ for 1 hr.

Fig.4.1 shows the XRD pattern of samples M1, M2 and M3, where, M1 is standard sample of pure ammonium heptamolybdate (AHM), M2 is the XRD pattern of the sample subjected to thermal decomposition of AHM, while M3 shows the thermal decomposition of AHM with the addition of magnesium (Mg) as a catalyst. Thermal decomposition of AHM (M2) in an autoclave at 800 $^oC$ for 1 hr at constant heating rate of 5 $^oC$/min shows presence of only $MoO_2$ in XRD pattern, which confirms that AHM decomposes to $MoO_3$ [1] which further reduces to $MoO_2$ in the presence of $NH_3$ [2] generated during the decomposition step of AHM [3]. However, the nitridation process has not emerged at this stage to form any of the nitride phase. Whereas, the addition of Mg as catalyst in AHM favors the reaction at 800 $^oC$ (M3) in forward direction. It not only enhances reduction of

AHM to $MoO_2$ but also allows hydrogen to diffuse into $MoO_2$ lattice and reduce it to molybdenum metal. This formation of Mo metal provides active sites for synthesis of $Mo_2N$ via nitridation process. Although the amount of nitride formed is very less as compared to Mo metal therefore the reaction temperature and time was varied.

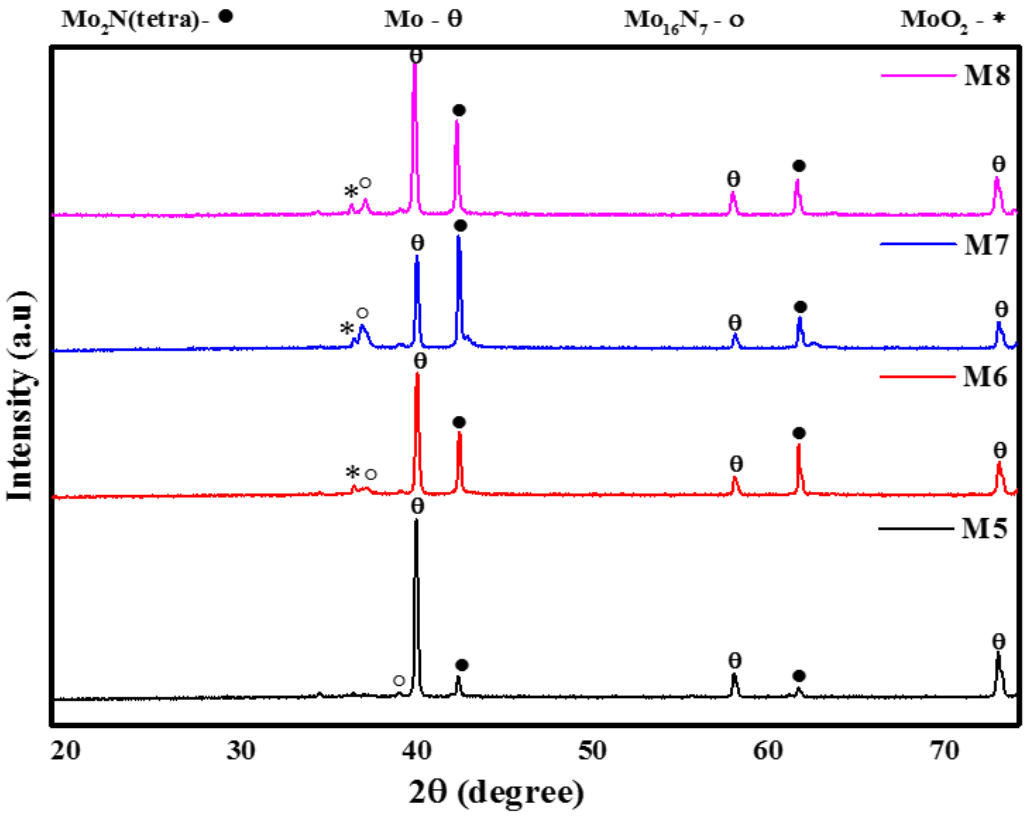


**Figure 4.2:** XRD patterns of samples synthesized at 500 $^oC$ (M5), 600 $^oC$ (M6), 700 $^oC$ (M7) and 800 $^oC$ (M8).

Fig.4.2 shows the XRD patterns of thermally decomposed of AHM for 10 hrs at different temperatures (500, 600, 700 and 800 $^oC$) as M5, M6, M7 and M8 in presence of magnesium. M5 shows the formation of Mo metal with little peaks of subnitride ($Mo_{16}N_7$) and nitride ($Mo_2N$) phase. The formation of subnitride indicates that the nitridation process has started but reaction temperature (500 $^oC$) is not sufficient to accomplish diffusion of N in Mo lattice. So the reaction temperature was increased from 500 $^oC$ to 800 $^oC$ to form $Mo_2N$. Increasing reaction temperature to 600 $^oC$ (M6) shows that the yield of β-$Mo_2N$ increases and Mo phase decreases. Further increase in temperature to 700 $^oC$ (M7) shows that impurity phase ($MoO_2$, Mo) are diminishing and the intensity of $Mo_2N$ phase increases as shown in Fig.4.2. Increasing temperature, thus, favors the reaction in forward direction

and enhances the nitridation of reduced $MoO_2$ and Mo phase. However, when the temperature is increased to 800 $^oC$, it resulted in decrease of β-$Mo_2N$ phase. This may be due to the fact that at high temperature (800 $^oC$), even a small variation in pressure inside autoclave results in the decrease in β-$Mo_2N$ phase [4]. This variation in pressure might have caused due to production of $NH_3$ and $H_2O$ as a reaction byproduct in each decomposition step of AHM. Therefore, the increase in pressure more than an optimum value may reduce the yield of nitride [5]. Thus, the probability of formation of $Mo_2N$ at 700 $^oC$ is more. This temperature seems to be the optimum temperature for formation of $Mo_2N$. The presence of impurity phase Mo and $MoO_2$ (very little amount) shows that the nitrogen content is not enough to form $Mo_2N$ completely. The decomposition of AHM in presence of Mg in an autoclave at different temperatures (500-700 $^oC$) does not provide sufficient nitrogen to form pure phase $Mo_2N$. However, the reduction process has accomplished at this stage.

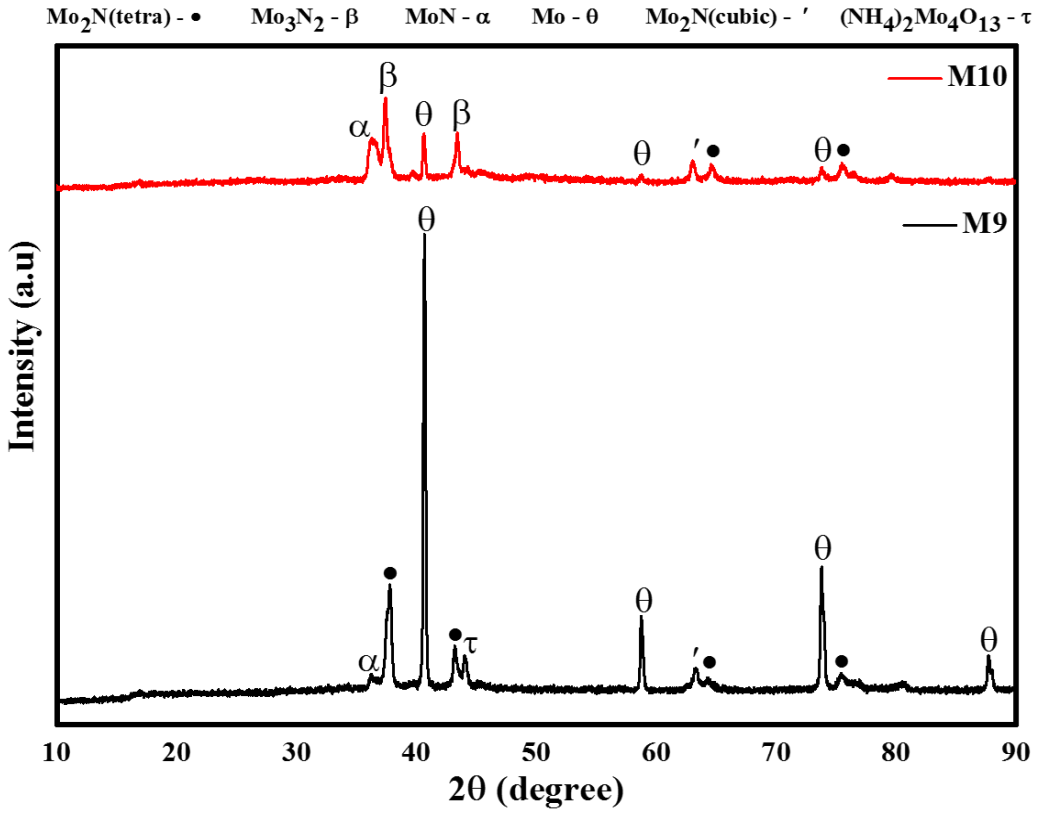


**Figure 4.3:** Effect of temperature 600 $^oC$ (M9) and 700 $^oC$ (M10) at constant holding time (10 hrs) with the addition of $NaN_3$.

To enhance the nitridation process sodium azide ($NaN_3$) was used as nitrogen source. Fig.4.3 shows the XRD patterns of samples synthesized at 600 $^oC$ and 700 $^oC$ labelled as M9 and M10, respectively for reaction time of 10 hrs. 1 g of $NaN_3$ as solid nitrogen source was added to a mixture of AHM and Mg to form $Mo_2N$. The results show that in sample M9, the most dominating phase is Mo metal along with other intermediate nitrides. The nitride phase formation increases in M9 as compared to M6 (Fig.4.2). But the reaction temperature of 600 $^oC$ is not sufficient enough to accomplish the reduction process due to presence of $(NH_4)_2Mo_4O_{13}$ phase. The increase in reaction temperature to 700 $^oC$ (M10) shows the decrease in intensity of Mo while the nitride phase formation increases. This may be due to higher affinity of nitrogen diffusion inside the Mo at higher temperature.

### 4.1 (B) Effect of holding time on the synthesis of nano molybdenum nitride

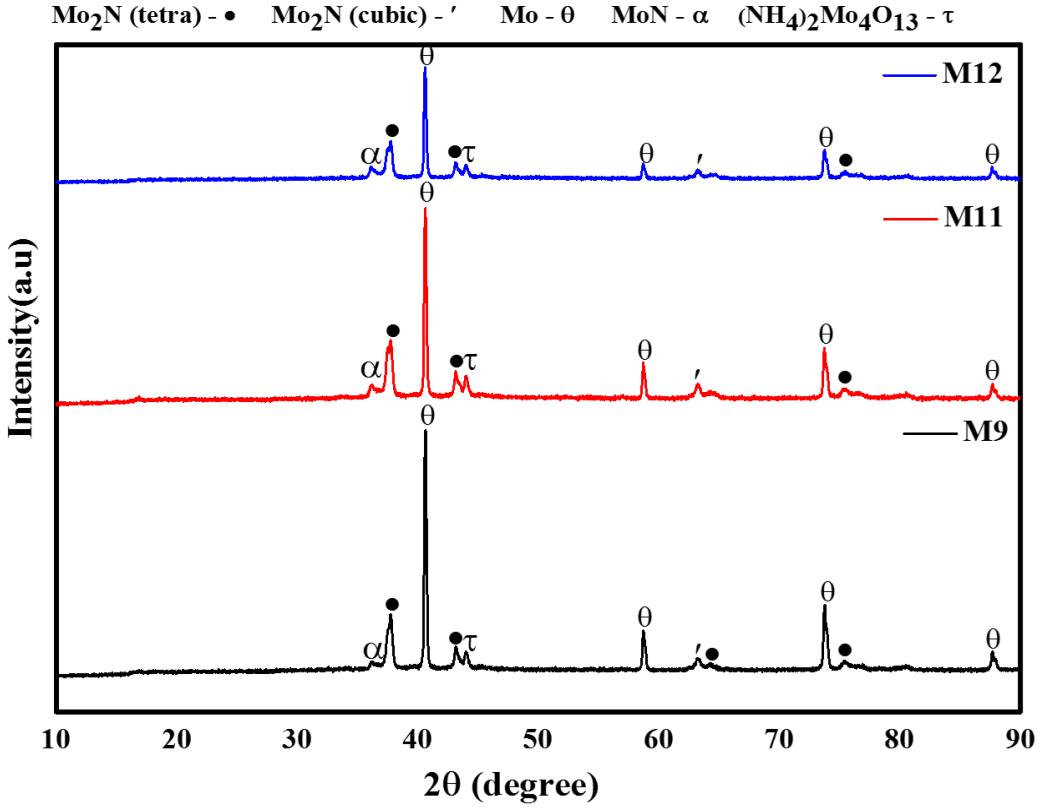


**Figure 4.4:** Effect of holding time at 600 $^oC$, 10 hrs (M9), 15 hrs (M11) and 20 hrs (M12).

Fig.4.4 shows the XRD pattern of samples (M9, M11 and M12), synthesized at constant temperature of 600 $^oC$ for different holding times (10, 15 and 20 hrs), respectively. Increasing the reaction time from 10 to 20 hrs shows the decrease in peak intensity of Mo

metal. The phase formation of $Mo_2N$ increases with increase in reaction time. However, it does not show much effect on peak intensity of $Mo_2N$ phases with increasing time from 15 to 20 hrs. The presence of $(NH_4)_2Mo_4O_{13}$ phase shows that 600 $^oC$ is not an optimum temperature for synthesis of $Mo_2N$ even if reaction time is increased.

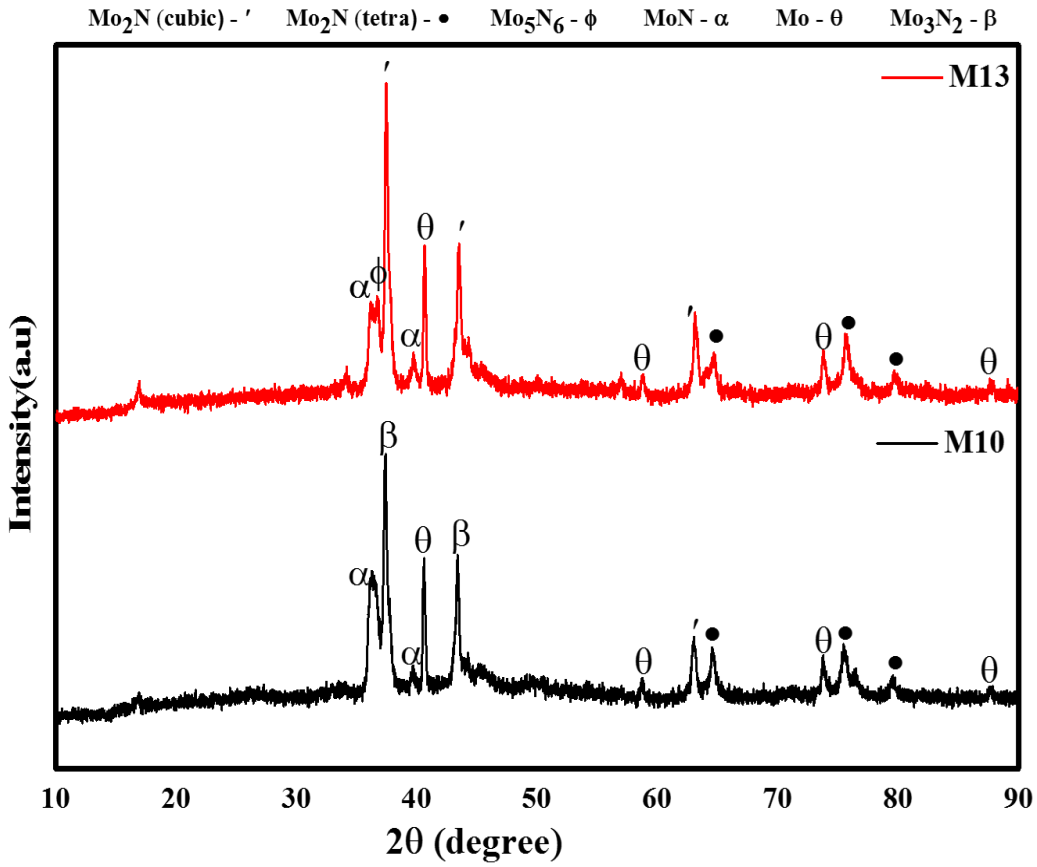


**Figure 4.5:** Effect of holding time 10 hrs (M10) and 12 hrs (M13) at constant temperature (700 $^oC$).

Fig.4.5 shows the XRD pattern of samples M10 and M13 synthesized at constant temperature (700 $^oC$) for different holding times 10 and 12 hrs, respectively. It can be observed that in M10, intermediate phase $Mo_3N_2$ is formed due to incomplete nitridation. Whereas, stable c-$Mo_2N$ phase was predominant when the sample was heated for 12 hrs. In both the synthesized samples, intermediate phases of nitrides ($Mo_3N_2$, MoN and $Mo_5N_6$) and Mo metal were observed along with $Mo_2N$. The results reveal that $MoO_2$ phase is converted to intermediate nitrides at 700 $^oC$. This conversion of oxide to intermediate

nitride shows that nitridation process prevails but still is not accomplished due to lack of nitrogen content.

### 4.1 (C) Effect of variation in quantity of Sodium azide ($NaN_3$) on the synthesis of nano molybdenum nitride

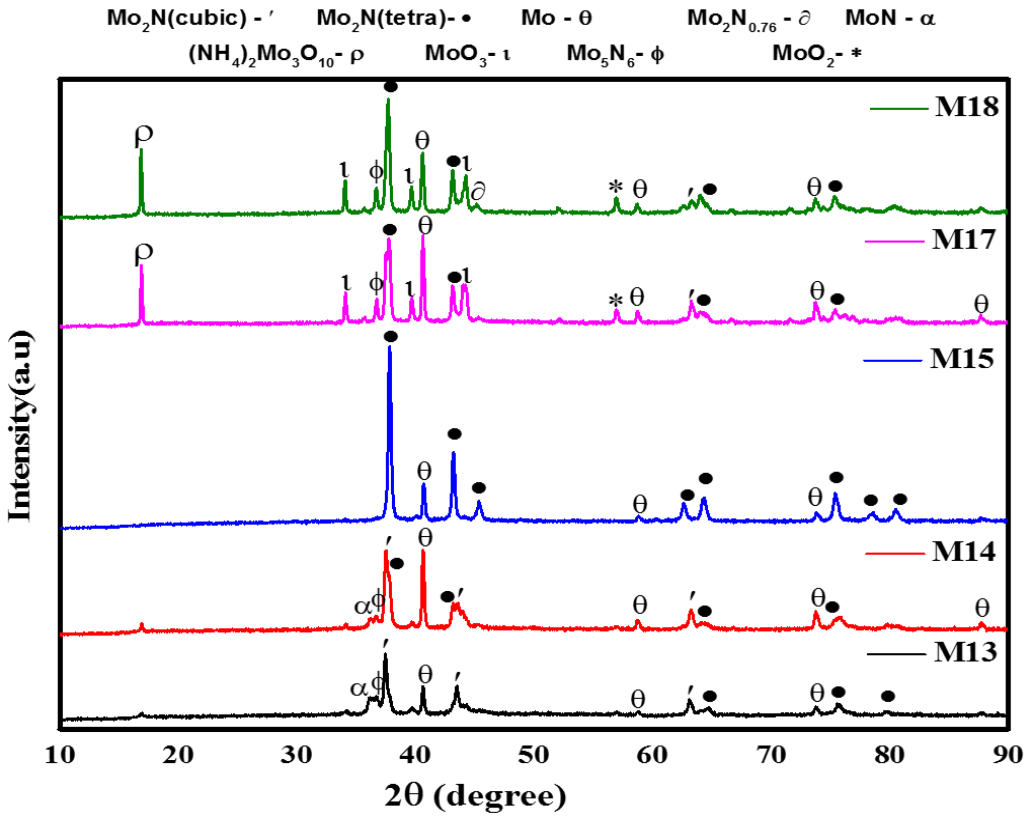


**Figure 4.6:** Effect of variation of $NaN_3$, 1.0 g (M13), 1.5 g (M14), 2.0 g (M15), 2.5 g (M17) and 3.0 g (M18).

To verify the effect of nitrogen content, different amount of $NaN_3$ was added to mixture of AHM and Mg at particular temperature and time. Fig.4.6 shows the samples M13, M14, M15, M17 and M18 synthesized at 700 $^oC$ for 12 hrs with varying quantities of $NaN_3$, ie., 1.0 g, 1.5 g, 2.0 g, 2.5 g and 3 g respectively. From the XRD pattern it is evident that with the increase in $NaN_3$ from 1.0 g to 2.0 g, the nitridation process is almost accomplished. Increase in $NaN_3$ from 1.0 to 1.5 g increases the formation of c-$Mo_2N$, with Mo as dominant phase. The pattern also contains impurity phase (MoN and $Mo_5N_6$). However, the $Mo_2N$ phase formation increases drastically at 2.0 g $NaN_3$ as shown in Fig.4.6. It only contains little amount of Mo metal. The formation of β-$Mo_2N$ with a very few peaks of Mo shows that reaction proceeds fast in forward direction with increase in $NaN_3$ from 1.5 to 2.0 g.

Increase in $NaN_3$ from 2.0 to 2.5 g in M15 and M17, respectively shows decrease in yield of β-$Mo_2N$. The same effect was observed with increasing the azide content from 2.5 to 3.0 g. However, it leads to formation of many intermediate phases. Therefore, it can be concluded that with the increase in the $NaN_3$ quantity upto 2.0 g shows conversion of oxides and the intermediate nitride phases and finally into a single phase β-$Mo_2N$ along with minor peaks corresponding to Mo metal. But further increase in quantity of $NaN_3$ in the autoclave generates high pressure which leads the formation of many phases of metal nitrides [6]. Marin- ayral and his co-workers reported that although the increase in nitrogen pressure helps in the formation of more nitrides, but, if the nitrogen pressure is exceeded more than a particular value, then there is a decrease in nitride content. This is because of mechanical strains which are the results of plastic deformation of metal grains at very high pressure [5]. Moreover, the presence of sub-nitrides and metals have been reported due to incomplete reaction. The presence of Mo metal with $Mo_2N$ in sample M15 is in accordance with the reported data [6]. Moreover, Roy and his co-workers predicted that temperature about 700 $^oC$ is sufficient for the formation of molybdenum nitride [7].

### 4.1 (D) Effect of variation in quantity of Ammonium heptamolybdate tetrahydrate (AHM) on the synthesis of nano molybdenum nitride

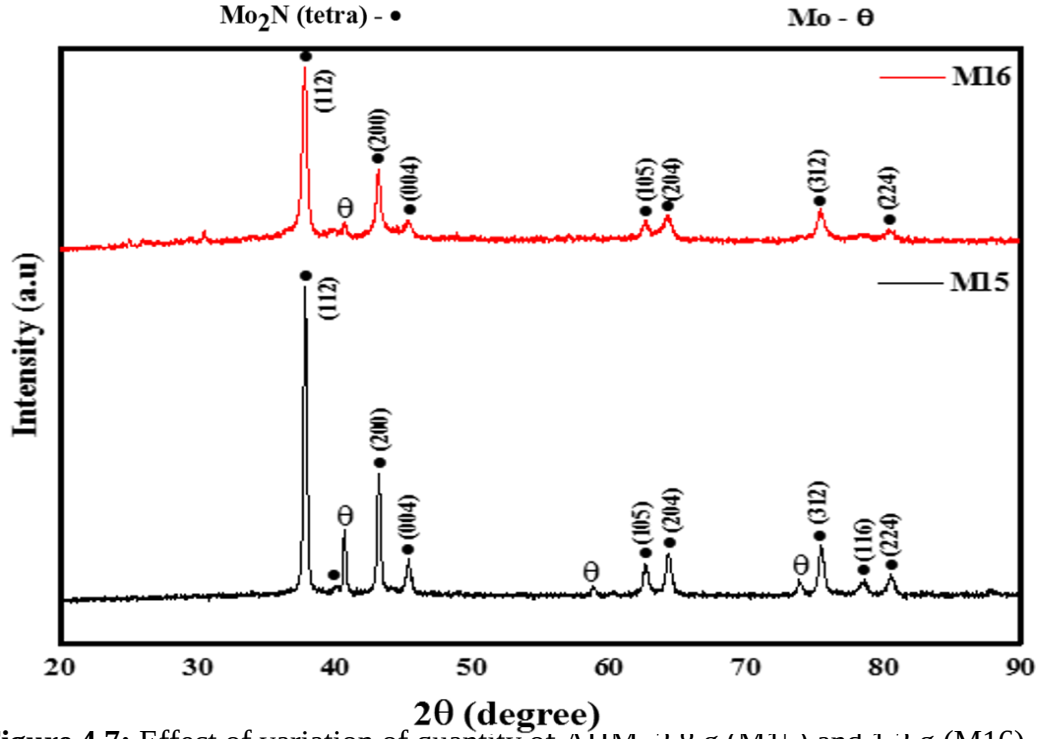


**Figure 4.7:** Effect of variation of quantity of AHM, 2.8 g (M15) and 1.2 g (M16).

Fig.4.7 shows the formation of single phase $Mo_2N$ with the variation in quantity of AHM keeping the Mg and $NaN_3$ (2 g) quantities same. Here, M15 and M16 represents the samples with 2.8 g and 1.2 g of AHM respectively, heated at 700 $^oC$ for 12 hrs. It can be seen that for less quantity of AHM more pure phase of β-$Mo_2N$ is obtained. The results predict that this molar ratio (0.001:0.03) of AHM to $NaN_3$ is optimum for formation of $Mo_2N$ at a given temperature and time condition. In sample M16 as shown in Fig.4.7 all peaks corresponds to tetragonal-$Mo_2N$ matched with ICDD pattern 01-075-1150 showing the peaks at 2 theta (37.77), (43.09), (75.32), (64.22), (45.31), (62.64) and (80.44) corresponding to (112), (200), (312), (204), (004), (105) and (224) planes.

## 4.2 Crystallite size, lattice parameter and strain analysis

The line profile technique was used for calculation of crystallite size and strain in samples. The determination of Bragg peak position (2θ) and full width half maximum (FWHM) was done using Gaussian peak function, which is more pragmatic and stable distribution function in comparison to other functions for the calculation of crystallite size ($D$) and strain (ε). The best curve fitting of peaks were taken into account and shown in Fig.4.8 (a) and 4.9 (a).

For the calculation of crystallite size, Scherrer method was used as it is the most reliable and versatile approach. According to this method the Bragg's peak is related to crystallite size as:

$$\boldsymbol{D = {k\lambda}/{\beta_D \cos\theta}} \quad \text{(iii)}$$

where, λ is X-ray wavelength (0.15406 nm); θ is the Bragg's angle; D is crystallite size But the breadth of Bragg's peak ($\beta_D$) is a result of combination of sample dependent effects and instrumental dependent effects [8]. So, a correction corresponding to each and every diffraction peak of sample was required. This instrumental peak broadening was calculated for standard Si sample. The corrected peak broadening $\beta_D$ is calculated as:

$$\boldsymbol{\beta_D = \left[\left(\beta^2_{measured}\right) - \left(\beta^2_{Instrumental}\right)\right]^{1/2}} \quad \text{(iv)}$$

On combining equation (iii) and (iv), we get

$$\boldsymbol{\cos\theta = {k\lambda}/{D}\left({1}/{\beta_D}\right)} \quad \text{(v)}$$

where, $k$ is shape factor with a value 0.9394.

A graph between $^{1}/_{\beta_D}$ and cos $\theta$ along X and Y-axis respectively gives a straight line. The slope of the line corresponds to $^{k\lambda}/_{D}$. Fig 4.8 (b) and Fig 4.9 (b) shows the linear fit of eq. (v) and the crystallite size was calculated for the corresponding slopes. Also, the unit cell parameters a, b and c for tetragonal system (a = b ≠ c) were calculated using the relationship between interplanar spacing'd' and (hkl) values:

$$^{1}/_{d^2} = {}^{1}/_{a^2}\,(h^2 + k^2) + {}^{1}/_{c^2}\,(l^2) \qquad \text{(vi)}$$

**Table 4.2:** Values of lattice parameters for samples M15 and M16.

| Sample | a = b (Å) | c (Å) |
|---|---|---|
| M15 | 4.188 | 7.998 |
| M16 | 4.185 | 7.998 |

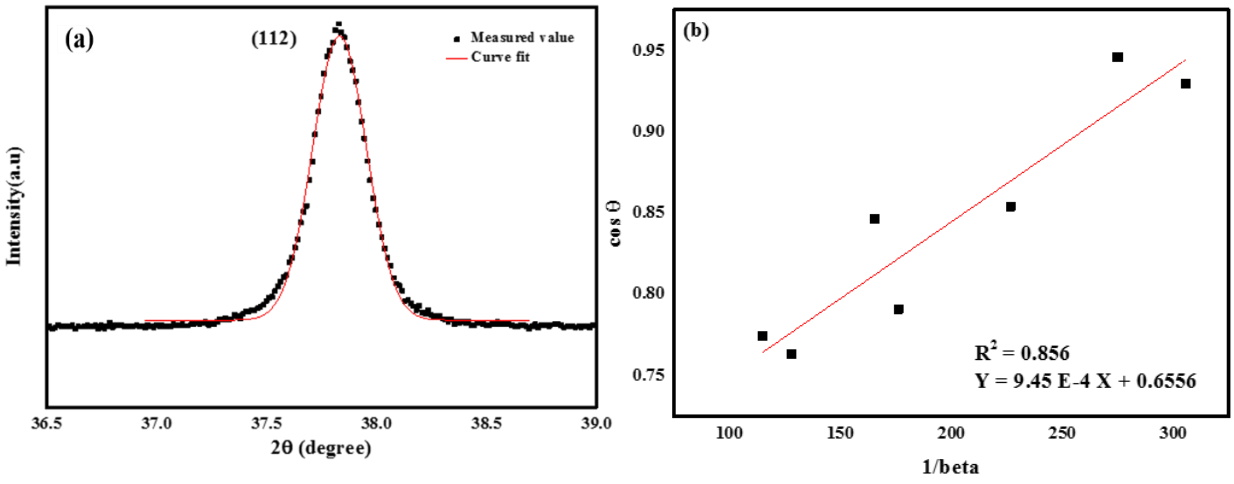


**Figure 4.8:** (a) Peak fitting for sample M15 using Gaussian function (b) Linear fit of sample M15.

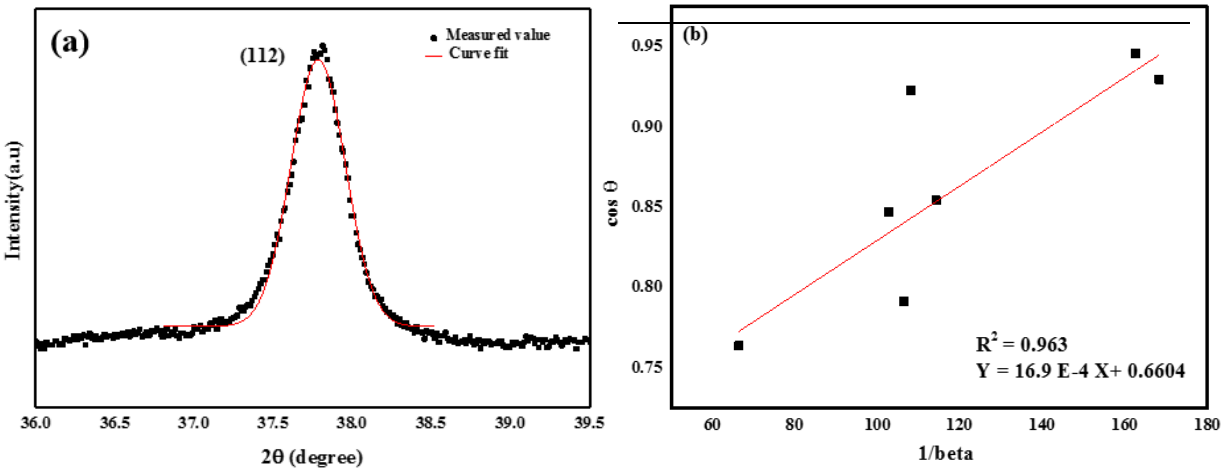


**Figure 4.9:** (a) Peak fitting for sample M16 using Gaussian function (b) Linear fit of sample M16.

Williamson-Hall (W-H) method is used to calculate crystallite size as a function of stress, strain and energy density. While, Scherrer method relates the crystallite size to the peak broadening by 1/ cos θ dependency, W-H method shows the tan θ dependency. This method basically comprises of three models:

1. UDM (uniform deformation model)
2. USDM (uniform stress deformation model)
3. USEDM (uniform deformation energy density model)

Out of the three, UDM model was used to measure the crystallite size and stress induced in samples M15 and M16. According to UDM model, strain (ε) and FWHM (β) follows a direct relationship as:

$$\boldsymbol{\varepsilon = {\beta_{hkl}}/{4\tan\theta}} \quad \text{(vii)}$$

as the particle size and strain both contribute independently to the line broadening. So,

$$\boldsymbol{\beta_{hkl} = \beta_D + \beta_\varepsilon} \quad \text{(viii)}$$

Substituting $\beta_D$ from eq. (iii), we get

$$\boldsymbol{\beta_{hkl} = {k\lambda}/{D\cos\theta} + 4\varepsilon\tan\theta} \quad \text{(ix)}$$

On rearranging we get,

$$\boldsymbol{\beta_{hkl}\cos\theta = {k\lambda}/{D} + 4\varepsilon\sin\theta} \quad \text{(x)}$$

The graph between $4\sin\theta$ along x-axis and $\beta_{hkl}\cos\theta$ along y-axis gives a straight line where slope of the equation gives the amount of strain (ε) produced in the sample and

intercept $k\lambda/_D$ gives the crystallite size ($D$). Table 4.3 shows the crystallite size (from Scherrer method and W-H analysis) along with the corresponding strain in the samples.

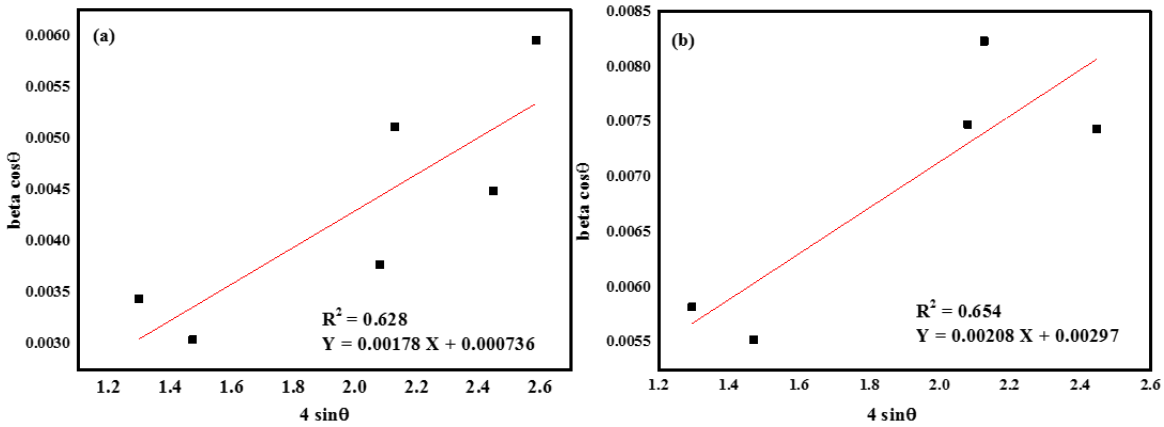


**Figure 4.10:** Williamson-Hall analysis using USM for M15 and M16.

**Table 4.3:** The crystallite size and strain in samples M15 and M16.

| Sample | Scherrer method | Uniform deformation table | |
|---|---|---|---|
| | Crystallite size (D) (nm) | Crystallite size (D) (nm) | Strain (ε) |
| M15 | 153.14 | 196.61 | 4.45 E-4 |
| M16 | 85.63 | 48.72 | 7.02 E-4 |

From table 4.3, it can be concluded that amount of precursor has a dependency on the strain of particles. The volume fraction of β-$Mo_2N$ is more and the crystallite size is less in case of M16 than in sample M15. However, higher strain in M16 can be correlated to the broadening of XRD peaks in Fig.4.7.

## 4.3 Field emission scanning electron microscopy (FE-SEM) analysis

The morphological features of β-$Mo_2N$ nanoparticles were studied by FE-SEM. Fig.4.11 (a) and (c) shows the large agglomeration of as prepared sample M15 and M16, respectively. However, the Fig.4.11 (b) and (d) shows the flake or platelet morphology [9] of M15 and M16.

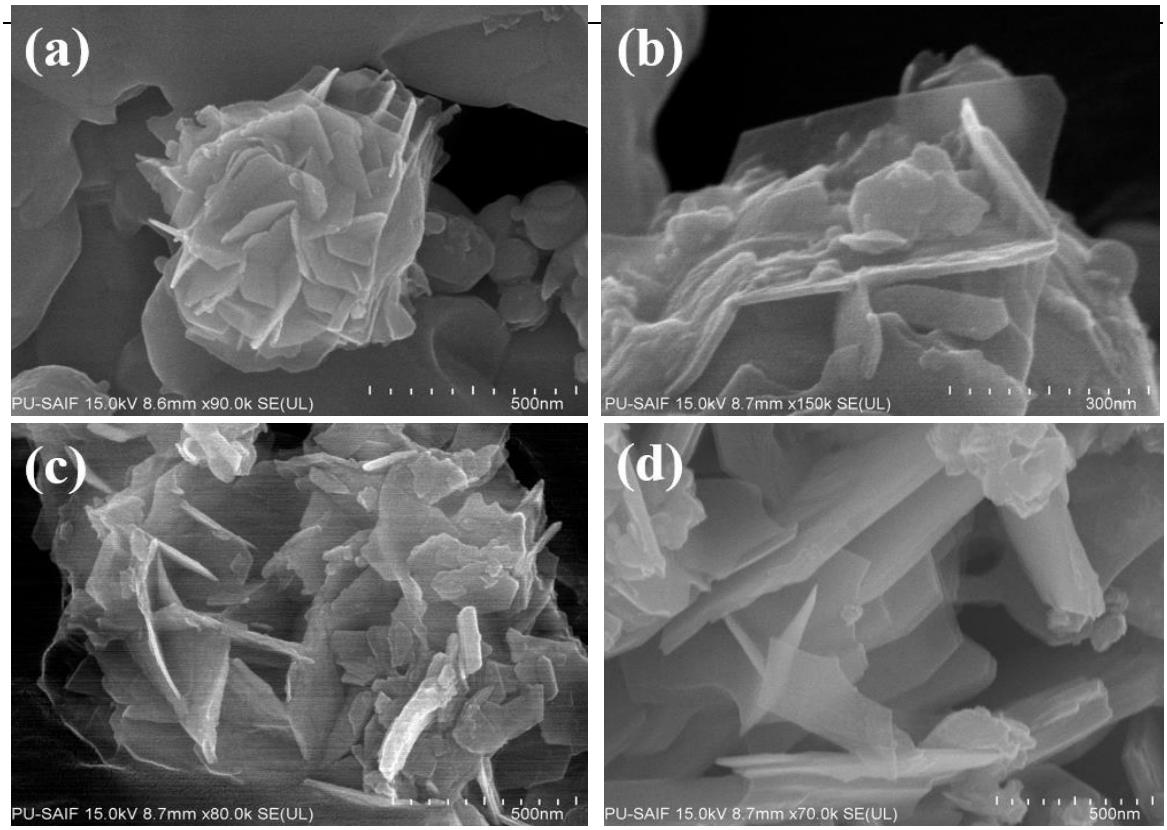


**Figure 4.11:** FE-SEM images of sample M15 (a,b) and M16 (c,d) showing platelet morphology.

## 4.4 High-resolution transmission electron microscopy (HR-TEM) analysis

To investigate the crystal structure, particle size and morphology HR-TEM was done. The TEM micrographs of samples M15 (Fig 4.12a) and M16 (Fig 4.12b) shows the large agglomeration of nano-particles [10]. In Fig 4.12 (b) the flake/plate like morphology of prepared β-$Mo_2N$ nanoparticles can be distinctly seen.

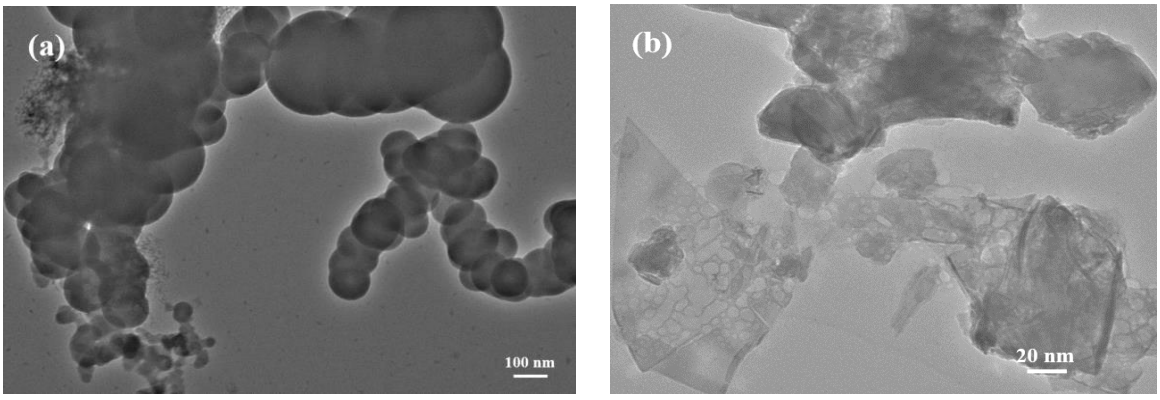


**Figure 4.12:** TEM micrograps of (a) M15 and (b) M16 samples.

The TEM micrographs as in Fig.4.12 clearly shows that there is a broad and random distribution of particle size. Therefore, it is necessary to plot the particle frequency against the logarithmic size to calculate the average size of nanoparticles. For log-normal probability distribution following calculations were done:

$$\boldsymbol{F(x) = \frac{1}{x_i.\sigma.(2\pi)^{1/2}}\, e - \left\{\frac{(\log(x_i)-\mu)^2}{2\sigma^2}\right\}} \quad \text{(xi)}$$

where, $F(x)$ is the log-normal distribution of particle size, $x_i$ is the particle size of i$^{th}$ particle, μ is mean and $\sigma$ is standard deviation of particle size.

$$\mu = \frac{\Sigma \log(x_i)}{\Sigma\, n_i} \qquad and \qquad \boldsymbol{\sigma = \left(\frac{\Sigma\,(\log(x_i)-\mu)^2}{\Sigma\, n_i}\right)^{1/2}} \quad \text{(xii)}$$

here, $n_i$ are the total number of particles.

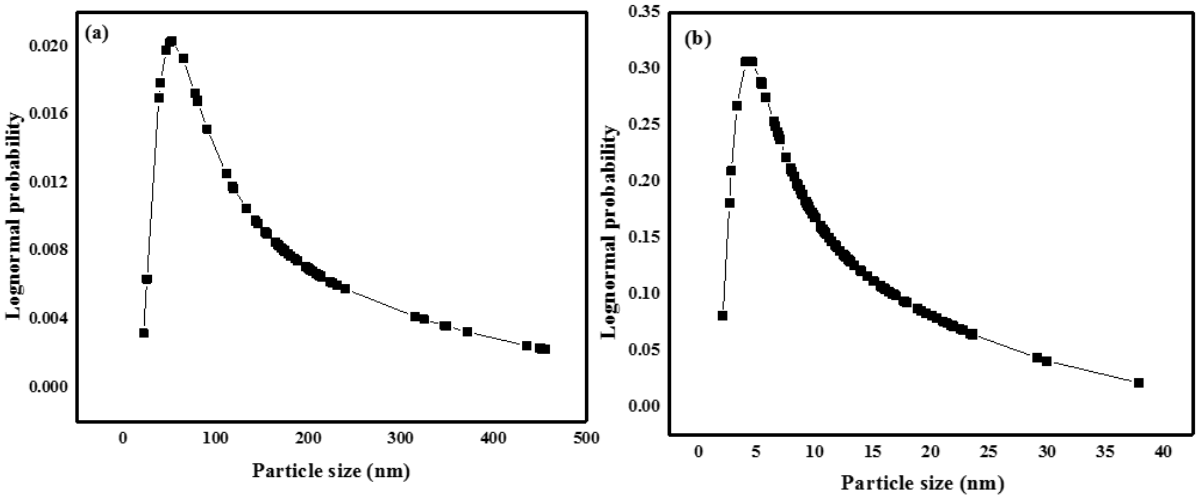


**Figure 4.13:** Log-normal probability distribution of β-$Mo_2N$ (a) M15 and (b) M16.

Fig.4.13 (a) shows the log-normal probability distribution of sample M15 which clearly shows that the average particle size of nanoparticles is in the range of 80-90 nm while Fig.4.13 (b) shows that of average particle size of sample M16 in range of 4-7 nm.

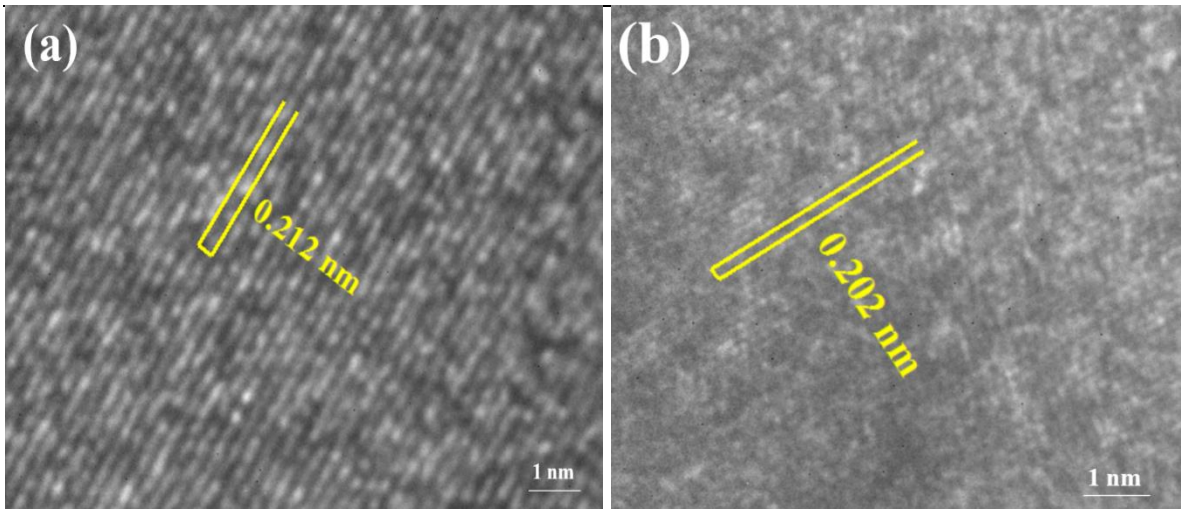


**Figure 4.14:** Shows the lattice fringes of β-$Mo_2N$ nanoparticles (a) shows the lattice fringe of plane (200) of M15 sample and (b) shows the lattice fringe of plane (004) of M16 sample.

## 4.5 Formation mechanism of molybdenum nitride

The numerous phenomena occurring inside the autoclave during heating and cooling process leads to the understanding of reaction mechanism for the synthesis of molybdenum nitride nanopowders. Initially, (AHM) was taken as a source of both molybdenum and nitrogen. The thermal decomposition of ammonium heptamolybdate (AHM) in an autoclave results in the formation of $MoO_2$ as the product phase at 800 $^oC$ for 1 hr. Kovacs and coworkers [3] described that thermal decomposition of $(NH_4)_6Mo_7O_{24}.4H_2O$ in both air and nitrogen atmosphere transforms $MoO_3$ yielding ammonia ($NH_3$) and water ($H_2O$) as reaction byproducts. To analyze the reaction mechanism in the present study, thermo-gravimetric analysis (TGA) of starting precursor (AHM) was done in nitrogen atmosphere in the temperature range of room temperature to 1000 $^oC$. The results obtained in TG analysis is shown in Fig.4.15. AHM decomposes to $MoO_3$ in three steps releasing both $NH_3$ and $H_2O$ in each step of decomposition [11]. The calculated mass loss due to release of $NH_3$ and $H_2O$ is in accordance with the observed mass loss as shown in Fig4.15. $(NH_4)_8Mo_{10}O_{34}$, $(NH_4)_2Mo_4O_{13}$ and $MoO_3$ were formed with the mass loss of 6.6 %, 4.2 % and 8 % respectively, at three decomposition steps with the release of $NH_3$ and $H_2O$. This decomposition of AHM can be shown as:

Step (a). $10(NH_4)_6Mo_7O_{24}.4H_2O \longrightarrow 7(NH_4)_8Mo_{10}O_{34} + 4NH_3 + 42H_2O$ (xiii)

Step (b). $2(NH_4)_8Mo_{10}O_{34} \longrightarrow 5(NH_4)_2Mo_4O_{13} + 6NH_3 + 3H_2O$ (xiv)

Step (c). $(NH_4)_2Mo_4O_{13} \longrightarrow 4MoO_3 + 2NH_3 + H_2O$ (xv)

TG analysis of AHM in nitrogen atmosphere at 800 $^oC$ shows the formation of $MoO_2$ with the mass loss of about ~15 % with release of $H_2O$ and $NH_3$. This shows that $MoO_3$ so produced is reduced to $MoO_2$ in nitrogen atmosphere. The formation of $MoO_2$ in an autoclave at 800 $^oC$ as given in Fig.4.1. is in accordance with the results obtained in TG analysis.

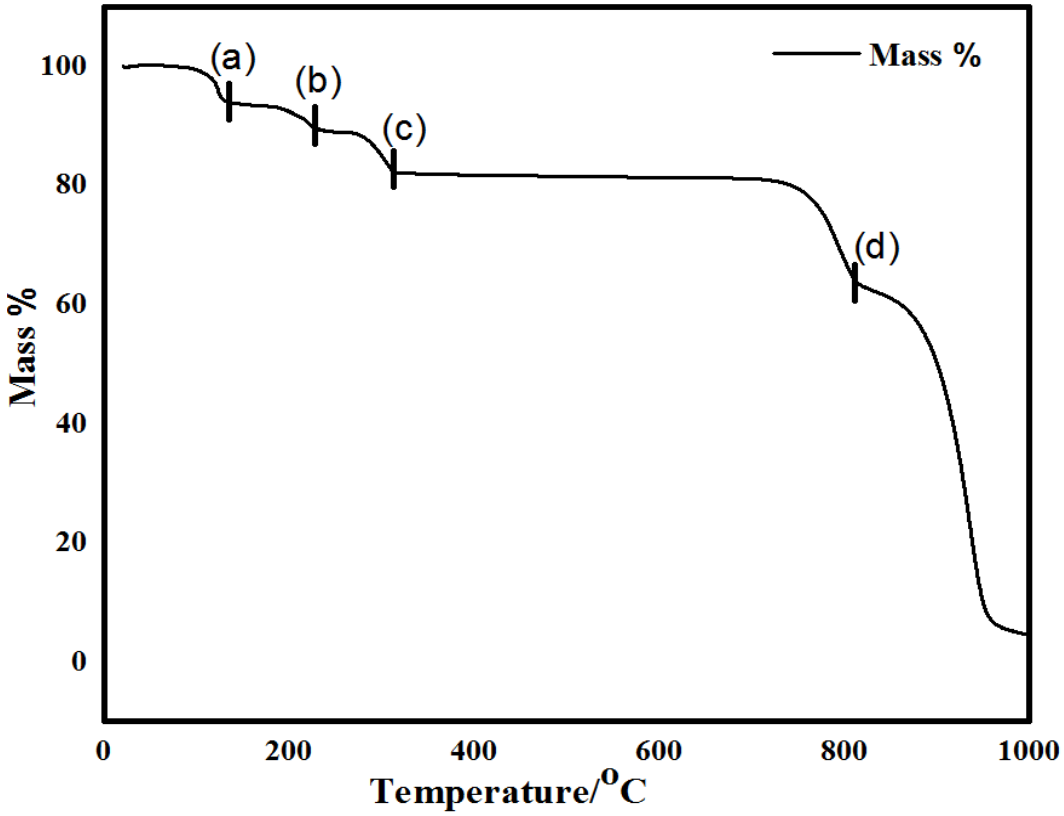


**Figure 4.15:** Thermogravimetric analysis of AHM in nitrogen atmosphere.

The following reactions might have taken place during the synthesis of $MoO_2$ from $MoO_3$:

$11MoO_3 + N_2 + NO_2 + 2NH_3 \longrightarrow 11MoO_2 + 5NO_2 + 3H_2O$ (xvi)

$9MoO_3 + ½\ N_2 + 2NH_3 \longrightarrow 9MoO_2 + 3NO_2 + 3H_2O$ (xvii)

$7MoO_3 + N_2 + 2NH_3 \longrightarrow 7MoO_2 + 2NO_2 + N_2 + 3H_2O$ (xviii)

$5MoO_3 + N_2 + H_2O + 2NH_3 \longrightarrow 5MoO_2 + NO_2 + 3/2N_2 + 4H_2O$ (xix)

$4MoO_3 + N_2 + 2H_2 \longrightarrow 4MoO_2 + NO_2 + 1/2N_2 + 2H_2O$ (xx)

$5MoO_3 + N_2 + H_2 \longrightarrow 5MoO_2 + 2NO_2 + H_2O$ (xxi)

$2MoO_3 + N_2 + NO_2 + 3NH_3 \longrightarrow 2MoO_2 + 3N_2 + 1/2H_2 + 4H_2O$ (xxii)

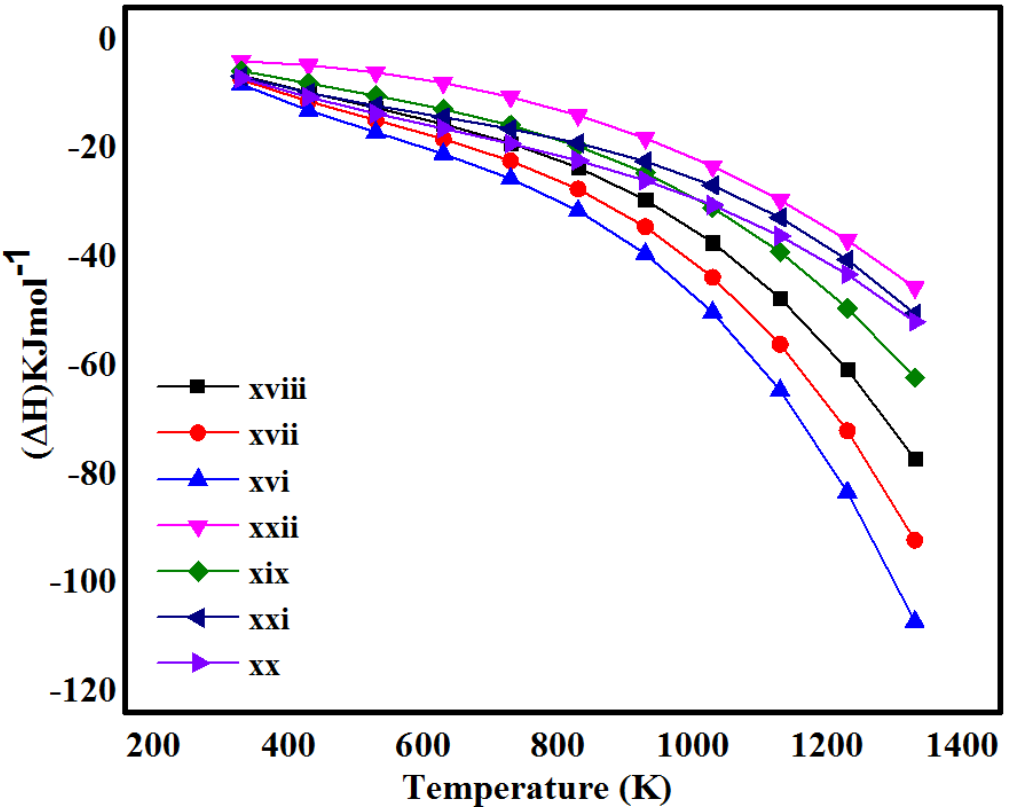


**Figure 4.16:** Variation in heat of formation with temperature for reduction of $MoO_3$ to form $MoO_2$.

Reaction (xvi) as shown in Fig.4.16. has the higher negative ΔH value among all the possible reactions. Therefore, it is the most feasible path for the formation of $MoO_2$ form $MoO_3$. It is observed that in present study AHM decomposes to $MoO_2$ at 800 $^oC$, which shows that only reduction of AHM takes place. However, no nitridation process occurs at this stage. Therefore to make reaction more feasible to synthesize $Mo_2N$, magnesium (Mg) was added as reducing agent. Mg being highly reactive reacts with oxygen inside the autoclve to form MgO as the catalyst [12]. Figure 4.1 (sample M3), shows the formation of Mo metal along with little amount of $Mo_2N$. This reveals that the addition of Mg enhances the reduction process in system. The presence of Hydrogen in the system also

helps in reduction process of $MoO_2$, as it has high coefficient of diffusion. Hydrogen enters in oxide and move along the grain boundaries of $MoO_2$ lattice, fragmenting it into smaller particles as shown in Fig.4.19. This leads to increase in surface area which further increases the rate of reaction. Following reaction pathways have been framed for reduction of $MoO_3$ to $MoO_2$ under nitrogen/hydrogen atmosphere in presence of Mg.

$$4MoO_2 + 2NH_3 + H_2 + 2Mg \longrightarrow 2Mo + Mo_2N + 2MgO + NO_2 + 4H_2O \quad \text{(xxiii)}$$

$$5MoO_2 + 2NH_3 + 7Mg \longrightarrow Mo + 2Mo_2N + 7MgO + 3H_2O \quad \text{(xxiv)}$$

$$6MoO_2 + 2NH_3 + N_2 + 2Mg + H_2 \longrightarrow 4Mo + Mo_2N + 2MgO + 3NO_2 + 4H_2O \quad \text{(xxv)}$$

$$3MoO_2 + 2NH_3 + H_2 + 2Mg \longrightarrow Mo + Mo_2N + 2MgO + 1/2N_2 + 4H_2O \quad \text{(xxvi)}$$

$$3MoO_2 + 3NO_2 + 7H_2 + 6Mg \longrightarrow Mo + Mo_2N + 6MgO + N_2 + H_2 + 6H_2O \quad \text{(xxvii)}$$

$$3MoO_2 + 2NO_2 + 5H_2 + 5Mg \longrightarrow Mo + Mo_2N + 5MgO + 1/2N_2 + 5H_2O \quad \text{(xxviii)}$$

$$3MoO_2 + 5NO_2 + 4H_2 + 16Mg \longrightarrow Mo + Mo_2N + 16MgO + 2NH_3 + N_2 + H_2 \quad \text{(xxix)}$$

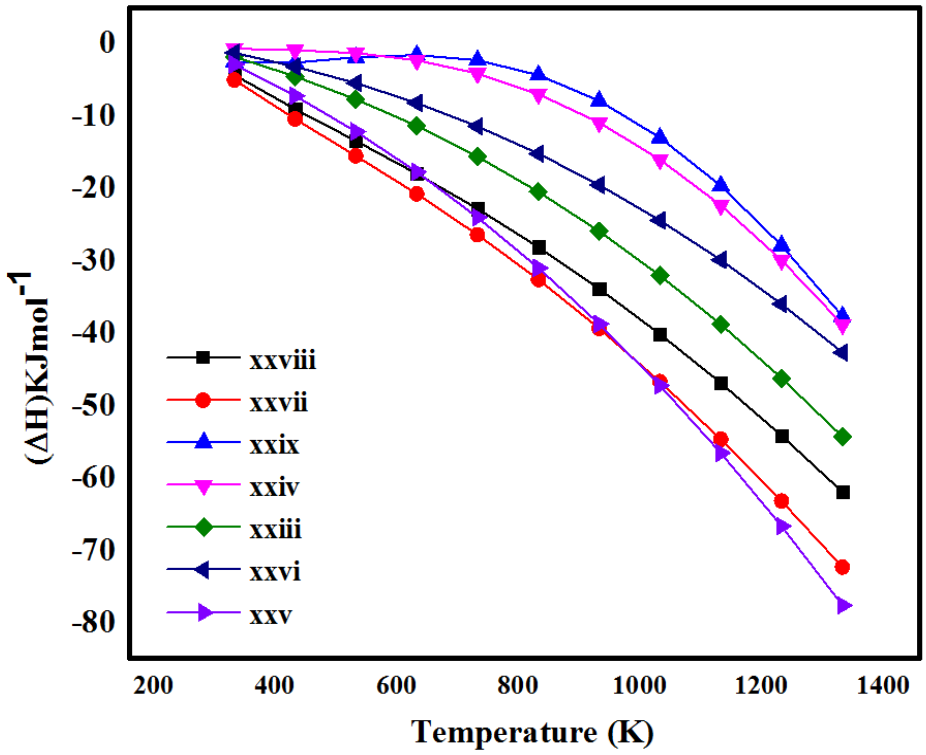


**Figure 4.17:** Variation in heat of formation with temperature for the reaction of $MoO_2$ in the presence of Mg to form Mo and $Mo_2N$.

Figure 4.17. shows that reaction (xxv) is most feasible in synthesizing Mo and $Mo_2N$ as it has higher -ΔH value. It also shows that nitridation process has started at this stage but is not sufficient to produce single phase $Mo_2N$. To enhance the nitridation process a nitrogen rich source sodium azide ($NaN_3$) was added in the system. $NaN_3$ decomposes in the temperature range of 240-365 $^oC$ producing nitrogen and sodium [13].

$$NaN_3 \longrightarrow Na + 3/2\ N_2 \qquad E_{th} = 34.54\ KJ\ mol^{-1} \quad (xxx)$$

The addition of $NaN_3$ favors the nitridation process leading to the formation of intermediate nitrides as seen in XRD results. All these subnitrides transforms to an almost single phase β-$Mo_2N$ at particular conditions of temperature and time. Inside the autoclave, not only temperature and time, but pressure also plays an important role. $NaN_3$ being high pressure producing compound increases the pressure inside autoclave, which affects the formation of $Mo_2N$. For that purpose an optimum amount of $NaN_3$ was added. Following reaction path way have been predicted for synthesis of $Mo_2N$ in presence of both Mg and $NaN_3$.

$$6MoO_2 + 2Mg + 2Na + 2NH_3 + N_2 \longrightarrow 4Mo + Mo_2N + 2MgO + Na_2O + 3NO_2 + 3H_2O \quad (xxxi)$$

$$6MoO_2 + 3Mg + 2Na + 4NH_3 + H_2O \longrightarrow 4Mo + Mo_2N + 3MgO + Na_2O + NO_2 + N_2 + 7H_2O \quad (xxxii)$$

$$3MoO_2 + 3Mg + 2Na + 4NH_3 + H_2 \longrightarrow Mo + Mo_2N + 3MgO + Na_2O + NO_2 + 7H_2 + N_2 \quad (xxxiii)$$

$$5MoO_2 + 8Mg + 4Na + N_2 \longrightarrow Mo + 2Mo_2N + 8MgO + 2Na_2O \quad (xxxiv)$$

$$5MoO_2 + 4Mg + 2Na + N_2 + 5H_2 \longrightarrow Mo + 2Mo_2N + 4MgO + Na_2O + 5H_2O \quad (xxxv)$$

$$5MoO_2 + 2Mg + 2Na + N_2 + 2NH_3 + H_2O \longrightarrow Mo + 2Mo_2N + 2MgO + Na_2O + 2NO_2 + 4H_2O \quad (xxxvi)$$

$$3MoO_2 + 8Mg + 2Na + 2NO_2 + H_2 \longrightarrow Mo + Mo_2N + 8MgO + Na_2O + 1/2N_2 + H_2O \quad (xxxvii)$$

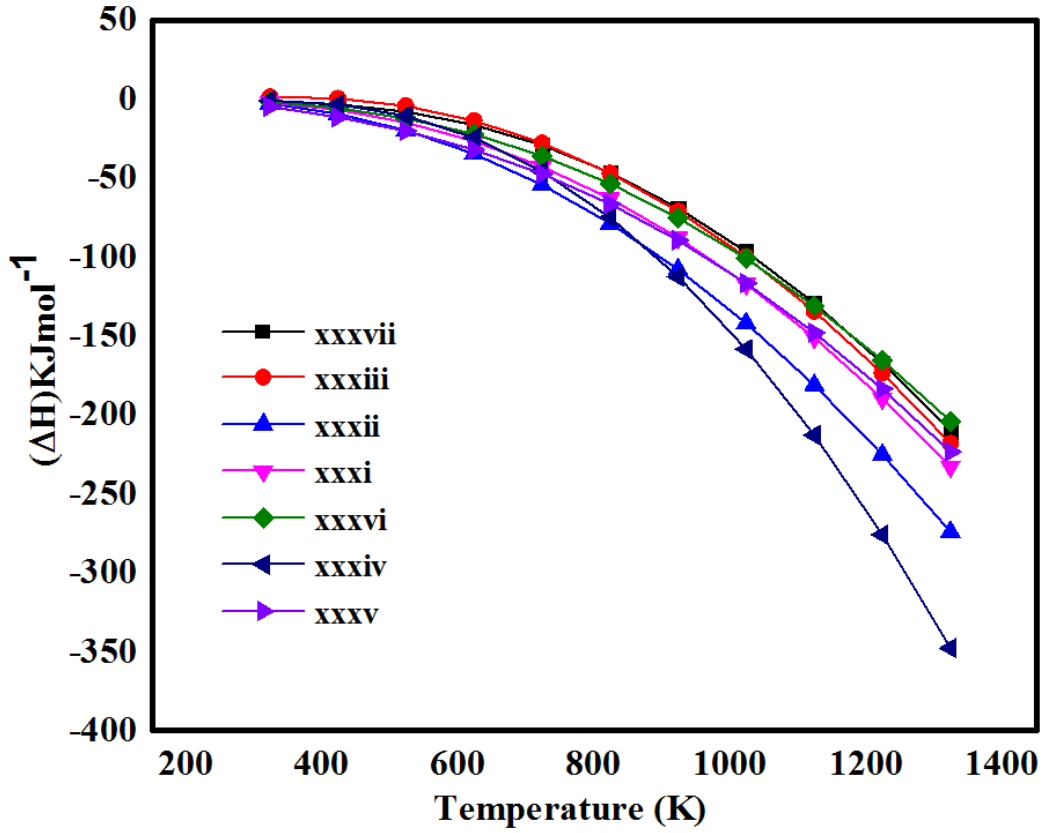


**Figure 4.18:** Variation in heat of formation with temperature for the reaction of $MoO_2$ in the presence of both Mg and $NaN_3$ to sythesize pure phase β-$Mo_2N$.

The reaction (xxxiv) having more negative ΔH variation with temperature is the most feasible reaction path for the formation of β-$Mo_2N$ as shown in Fig.4.18.

The addition of $NaN_3$ allows more nitrogen to diffuse in active sites provided by Mo lattice allowing the formation of subnitrides which further transforms to single phase β-$Mo_2N$ as the nitrogen content in the system increases [6]. In order to reduce the content of Mo produced in the system and increase the content of $Mo_2N$, optimization of reaction parameters was done to attain a single phase β-$Mo_2N$. The molar ratio of AHM to $NaN_3$ also affects the formation of $Mo_2N$. The optimum quantity of AHM (1.23g) shows the formation of $Mo_2N$ with a little amount of Mo present in the system as shown in schematic representation (Fig.4.19).

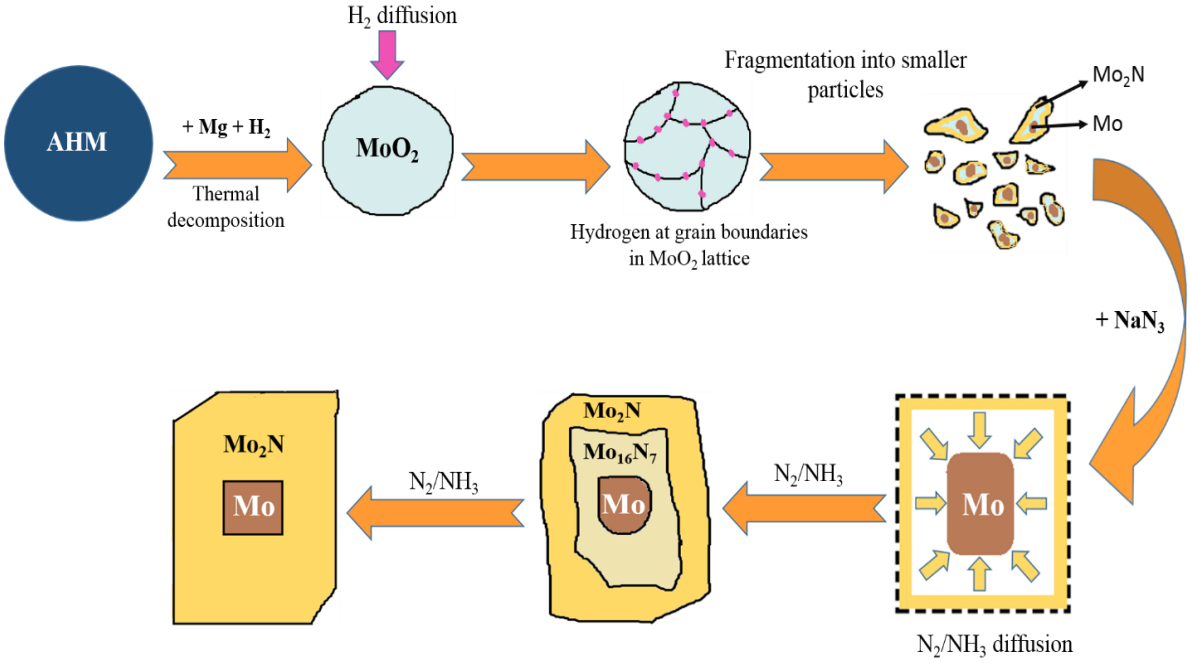


**Figure 4.19:** Schematic description of formation mechanism of molybdenum nitride nanopowders.

## 4.6 References


[1] Li X., Feng L., Zhang L., Dadyburjor D. & Kugler E., Alcohol synthesis over pre-reduced activated carbon-supported molybdenum-based catalyst, *Molecules*, **8,** 13-80, (2003).

[2] Kojima R. & Aika K., Molybdenum nitride and carbide catalyst for ammonia synthesis, *Applied Catal. A,* **29,** 141-147, (2001).

[3] Kovacs T.N., Hunyadi D., Lucene A. & Szilagyi I.M., Thermal decomposition of ammonium molybdates, *J. Therm. Anal. Calorim.,* **124,** 1013-1021, (2016).

[4] Wentorf R.H., Synthesis of cubic form of boron nitride, *The Journal of Chemical Phy.,* **34,** 809-812, (1961).

[5] Pascal C., Marin-Aryal R.M., Martinez F. & Tedenac J.C., Effect of nitrogen pressure on the combustion syntheis of titanium nitride, *High Pressure Research,* **18,** 331-338, (2000).

[6] O'Loughlin J., Wallace C.H., Knox M.S. & Kaner R.B., Rapid Solid-State Synthesis of tantalum, chromium, and molybdenum nitrides, *Inorg. Chem.*, **40,** 2240-2245, (2001).

[7] Roy A., Serov A., Artyushkova K., Brosha L., Atanassov P. & Ward L., Facile synthesis of high surface area Molybdenum Nitride and Carbide, *J . Solid State Chem.,* **228,** 232-238, (2015).

[8] Singla G., Singh K. & Pandey O.P., Williamson-Hall study on synthesized nanocrystalline tungsten carbide (WC), *Appl. Phys. A,* **113,** 237-242, (2013).

[9] Lizana F.C., Quero S.G., Perret N., Minsker L.K. & Keane M.A., β-Molybdenum nitride: synthesis mechanism and catalytic response in the gas phase hydrogenation of p-chloronitrobenzene, *Catal. Sci. Technol.,* **1,** 794-801, (2011).

[10] Cai P., Yang Z., Wang C., Gu Y. & Qian Y., A simple approach to synthesize $Mo_2N$ nanocrystals, *Chem. Lett.,* **34,** 1360-1361, (2005).

[11] Weinold J., Jentoft R. & Ressler T., Structural Investigation of the Thermal Decomposition of Ammonium Heptamolybdate by in situ XAFS and XRD, *Eur. J. Inorg. Chem.*, 1058-1071 (2003).

[12] Rameez A.M., Piyush S. & Pandey O.P., Thermal and structural studies of carbon coated $Mo_2C$ synthesized via in-situ single step reduction-carburization, *Sci. Reports*, **7,** 3518-3530, (2017).

[13] Verneker V.R.P. & Mohan K., Thermal decomposition of sodium azide, *Thermochimica Acta*, **21,** 375-380, (1977).

## 5. Conclusion

In this thesis work, nano powders of β-$Mo_2N$ has been synthesized, using reduction-nitridation route. Ammonium heptamolybdate tetrahydrate (AHM) $(NH_4)_6Mo_7O_{24}.H_2O$ was utilized as Mo and nitrogen source in the initial stages. The decomposition of AHM results in formation of $MoO_2$, which shows that reduction has accomplished at this stage. Mg as reducing agent and sodium azide ($NaN_3$) as nitrogen source enhanced the nitridation process to facilitate the formation of $Mo_2N$. The effect of reaction temperature and time plays an important role for the synthesis of $Mo_2N$. The reaction temperature of 700 °C and reaction of 12 hrs seems to be the optimum condition for synthesis of the β-$Mo_2N$ with little amount of Mo present. The molar ratio of AHM and $NaN_3$ plays a significant role for the synthesis of pure phase. The molar ratio of AHM to $NaN_3$ (0.001 : 0.03) results in formation β-$Mo_2N$ with two impurity peaks of low intensity corresponding to Mo. The molar ratio higher than optimum value shows de-nitridation process, which may be the result of extra pressure generated due to addition of $NaN_3$ inside the high pressure vessel autoclave. Crystallite size calculated with Scherer criterion for the M15 and M16 samples were 153 nm and 85 nm, respectively. FE-SEM results reveal that, the synthesized samples are highly agglomerated and have faceted/platelet and flake like morphology. TEM analysis of the synthesized samples showed the large agglomeration of particles with spherical to faceted morphology. HR-TEM showed the lattice fringes of width 0.212 nm and 0.202 nm corresponding to (200) and (004) planes of β-$Mo_2N$ for M15 and M16 samples.

## 6. Future scope

The nanopowders of β-$Mo_2N$ synthesized in the present work are potential candidates as high performance superconducting magnetic material and also as electrodes for energy storage devices. The resemblance of electronic structure of $Mo_2N$ with noble metal catalysts make these materials as promising alternate candidates to these costly catalysts. The catalytic activity and superconducting nature of these nitrides needs to be studied for various industrial applications.